

# Bivariate change point detection: joint detection of changes in expectation and variance

Michael Messer

Goethe University, Frankfurt

## Abstract

A method for change point detection is proposed. In a sequence of independent and piecewise identically distributed random variables we aim at detecting both, changes in the expectation as well as changes in the variance. We propose a statistical test for the null hypothesis of the absence of change points, and an algorithm for change point detection. For that we exploit the joint dynamics of the mean and the empirical variance in the context of bivariate moving sum statistics. The joint consideration helps to improve change point inference as compared to separate univariate approaches. We infer on the effects, i.e., on the strength and the type of the changes, with confidence. Non-parametric methodology allows for a high variety of data to be analyzed. A multi-scale aspect addresses the detection of complex patterns in change points and effects. We demonstrate the performance through theoretical results and simulations studies. A companion R-package `jcp` (available on CRAN) is discussed.

## 1 Introduction

The paper contributes to the field of change point detection which provides methods for the detection of structural breaks – change points – in stochastic sequences. Change point detection finds application in many areas of research, e.g., oceanographic sciences (Killick et al., 2010), neuroimaging (Aston and Kirch, 2012), telecommunication (Zhang et al., 2009), DNA sequencing (Braun et al., 2000), econometrics (Zeileis et al., 2010), to name a few. Change point problems are studied extensively in the literature. Thus, many aspects of statistical methodology are addressed, e.g., hypothesis testing, change point estimation, model complexity, computational feasibility, data structures, practical performance, etc., see the textbooks Basseville and Nikiforov (1993); Csörgö and Horváth (1997); Brodsky and Darkhovsky (1993); Chen and Gupta (2000); Brodsky (2017) or the review articles Aue and Horváth (2013); Jandhyala et al. (2013).

We study univariate piecewise i.i.d. sequences and provide a nonparametric method for the detection of change points which may occur on multiple time scales. Particularly, we aim at detecting changes in both the expectation and the variance. Among the vast literature, a

---

contact: [messer@math.uni-frankfurt.de](mailto:messer@math.uni-frankfurt.de)

Keywords: change point, joint detection, bivariate process, moving sum, `jcp`.

MSC subject classifications: 62G20, 62H15, 62H12.

The author is very grateful for valuable comments by Götz Kersting, Brooks Ferebee and Ralph Neininger.

Supported by the Priority Program 1665 of the DFG (grant number SCHN 1370/02-1, [www.dfg.de](http://www.dfg.de)).

great proportion concerns changes in expectation. We mention the nonparametric methods by Wolfe and Schechtman (1984); Horváth et al. (2008) or Eichinger and Kirch (2018), and regarding the detection of change points on multiple time scales we mention Spokoiny (2009); Fryzlewicz (2014); Matteson and James (2014) and Frick et al. (2014). The problem of detecting changes in the variance is less extensively studied. We mention the articles by Hsu (1977); Inclan and Tiao (1994); Chen and Gupta (1997); Whitcher et al. (2000); Killick et al. (2013) or Korkas and Fryzlewicz (2017). Combining both, changes in expectation and variance, we mention a paper by Pein et al. (2017) that aims at detecting changes in expectation by allowing the variance to change simultaneously. Vice versa, Gao et al. (2018) or Dette et al. (2015) study changes in variance allowing the expectation to vary smoothly.

In this paper we propose a bivariate method to jointly quantify change in expectation and in variance. We consider two moving sum processes: data is pointwise restricted to adjacent windows from which first the means, and second the empirical variances are compared. The first statistic is sensitive to changes in expectation and the second for changes in variance. See Figure 1 for an example of the two univariate processes (B,C) and their joint consideration (D), details explained later. Importantly, the bivariate nature helps to overcome flawed inference as compared to separate univariate approaches. Also it enables a straightforward interpretation of the types of changes (expectation, variance or both), as well as their strengths (effect size), while also controlling the error (confidence) about such statements. Methodologically, we construct first a statistical test for the null hypothesis of the absence of change points. Second, we propose an algorithm for change point detection which is run if the null hypothesis is rejected. The test and algorithm both rely on the asymptotics of the bivariate moving sum process.

We mention three upsides: first, theory is highly non-parametric which enables wide-ranging applicability. High performance is shown under different distributional assumptions, such as normal-, exponential- or gamma-distributed data. Second, multi-scale aspects are captured, meaning that the occurrence of fast as well as slow change points with different strengths of effects are tackled. Third, the method is ready to use. Theory is proven with all unknown quantities replaced by appropriate estimators. A companion R-package `jcp` (*joint change point detection*, Messer (2019)) is provided whose graphical output facilitates interpretation.

The paper is organized as follows: in Section 2 we give the ideas. In Section 3 we explain the model, and in Section 4 we introduce the moving sum statistics. We construct the test in Section 5 and discuss change point detection in Section 6. In Section 7 we give additional theory. In Section 8 practical aspects are considered: methodology is extended, the R-package `jcp` is discussed, extensive simulation studies are performed, and a real data example is shown. All proofs are given in the Appendix 10.

## 2 The idea of testing and change point detection

We discuss the idea of how moving sum processes are used to test the null hypothesis of absent change points, and for change point detection after rejection. Particularly, we motivate the bivariate aspect. For that consider three processes depicted and analyzed in Figure 1, differentiated in panels I, II, and III.

We consider  $T = 1000$  independent and normally distributed random variables (RVs), see red points in segments A and top D (coinciding). In panel I, there are no change points (i.i.d.).

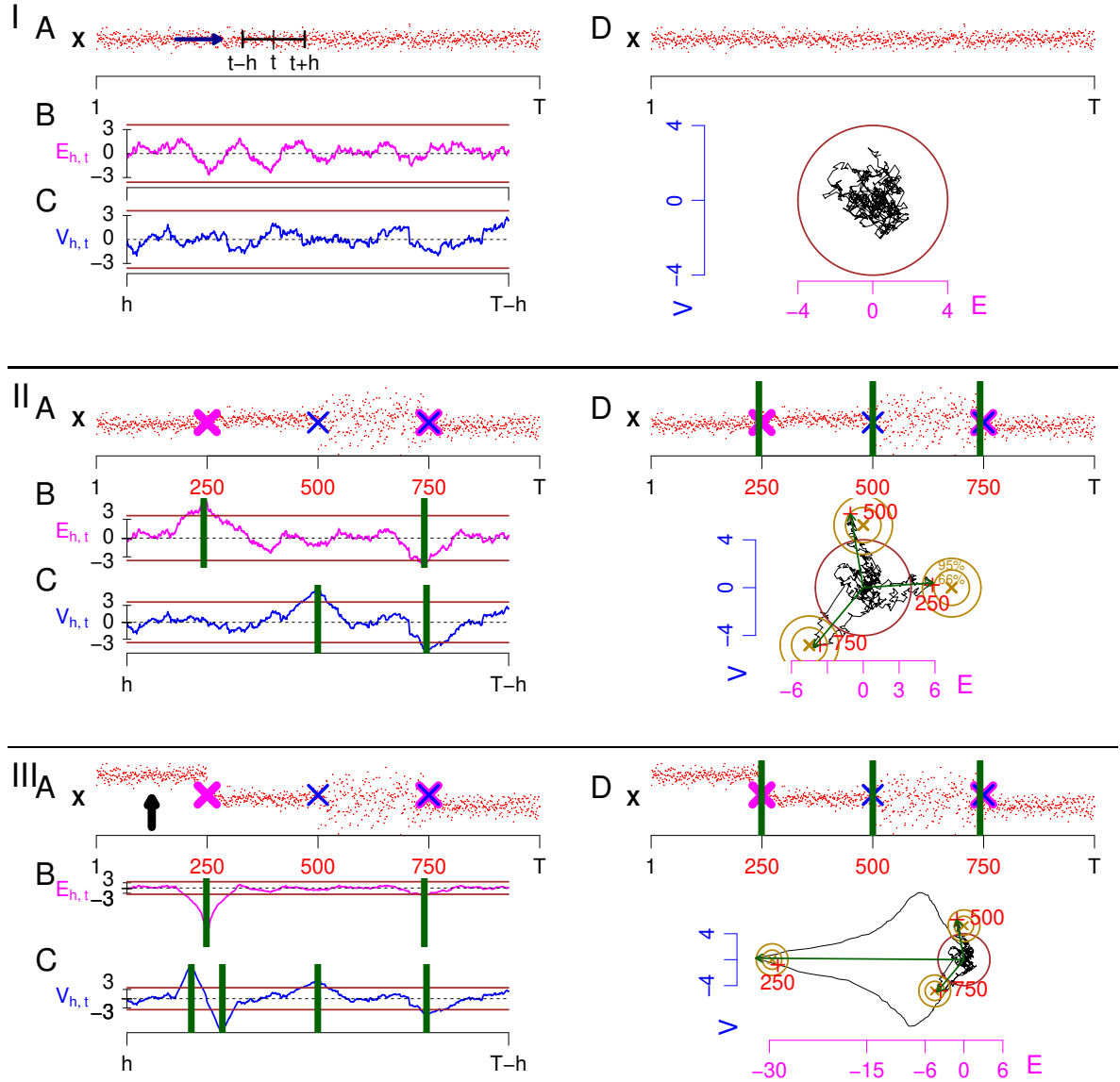


Figure 1: Univariate (B,C) and bivariate (D) change point detection.  $T = 1000$  normally distributed RVs (A), I: no change point. II, III: three change points at 250, 500, 750. Crosses mark the true change points, green bars their estimates. I: expectation 10, standard deviation 4. II: expectations 5, 10, 10, 3, standard deviations 4, 4, 12, 5, detected change points B: 243, 740, C: 500, 745, D: 243, 500, 742. III: expectations 30, 10, 10, 3, standard deviations 4, 4, 12, 5, detected change points B: 249, 740, C: 215, 285, 500, 745, D: 249, 500, 742.

In panels II and III there are three change points at 250, 500 at 750. In both panels II and III, the types of changes are the same: at time 250 there is a change in expectation (purple cross), at 500 there is an increase in variance (blue cross) and at time 750 there is a decrease in both, expectation and variance (purple and blue cross). The only difference between panel II and III is at 250: we find a small increase in expectation in II and a prominent decrease in expectation in III.

Moving sum processes are depicted in segments B, C, and D. Two adjacent windows of size

$h = 70$  (see panel IA) are shifted through time and statistics are evaluated locally from the RVs in the windows. The first statistics  $E_{h,t}$  (B, magenta) is Student's unpooled  $t$ -statistic, i.e., Welch's statistic, which compares the empirical means, see (5). It is sensitive to changes in expectation. The second statistic  $V_{h,t}$  (C, blue) similarly compares the empirical variances and is thus sensitive to changes in variance. In segment D we see a bivariate process (black) given by the joint statistic  $J_{h,t} := (E_{h,t}, V_{h,t})^t$ . If the windows do not overlap a change point then the two estimates from the left and right window typically resemble, resulting in a statistic close to zero. A strong deviation from zero indicates a change. We see brown rejection boundaries (B, C horizontal lines at  $\approx \pm 3.59$ , D circle with radius  $\approx 4$ . The boundaries are equal between the panels but appear different visually due to the scaling of the axes.) The idea is that the processes entirely lie within the boundaries with a predefined probability of  $1 - \alpha$ , here 95%, in case null hypothesis holds true, see panel I. If the boundaries are crossed at some point (II and III in B, C and D), the null hypothesis is rejected. The test is derived in detail in Section 5. After rejection, change points are estimated (green bars) via successive arg max estimation: find the largest deviation from zero, take the argument as a change point estimate, delete the process in the  $h$ -neighborhood of the estimate and repeat until the remaining process lies within the boundaries (also see Figure 5). In Figure 1 panel II inference is reasonable as in B the two changes in expectation were detected, in C the two changes in variance were detected, and in D all three change points were detected. In panel III expectation change detection succeeds in B, but unfortunately variance inference in C fails as there are also two changes in variance falsely estimated. This is caused by the prominent change in expectation. For an intuition, recall that the empirical variance is the mean squared deviation from the mean. Thus, when the expectation changes, this impacts the mean and thus the variance. Theoretically, this problem also appears in panel II, but as the change in expectation is small it practically does not affect the variance change detection. The other way around, changes in variance do practically not impact expectation change detection, intuitively because the mean is the first moment and not affected if only the second moment changes. Statements about robustness are subject to Section 7. One way to tackle false variance inference is to incorporate information about the changes in the expectation: if one correctly centers within the empirical variances then variance change detection will not systematically react falsely on changes in expectation. In the context of stochastic point processes this was analyzed in Albert et al. (2017). A second way of treating this problem is presented in this paper: the joint observation of both processes. In panel IIID we see that the problem is overcome in the bivariate procedure as there are three change points reasonably detected.

The golden dartboards in segment D represent the asymptotic distribution of  $J_{h,c}$  at the time of a true change point  $c$ . This distribution is bivariate normal, the golden cross marks the expectation and the circles the 66%- and 95%-contour lines, see Lemma 6.2. When the sliding windows run into a change point then  $(J_{h,t})_t$  starts an excursion approaching the center of the dartboard. The red crosses (+) mark  $J_{h,c}$  i.e., they can be interpreted as a realization from a dartboard. When the sliding windows trespass  $c$ , then the process returns to zero fluctuation. Glimpse at Figure 6 for the systematics of the excursions. The type and the strength of the change affect the systematic aspect of the excursion: if there is a change only in expectation, the process tends to leave the circle in horizontal direction, to right if there is an increase in expectation and to the left in case of a decrease. Indeed, at time 250 the dartboard is shifted only along the abscissa. In panel II it is found at the right side as there is an increase in expectation, and in panel III it is shifted left due to the decrease in expectation. Further, in panel III it lies far out since the change in expectation is strong. If there is a change only in

variance, the process systematically moves along the ordinate, upwards in case of an increase and downwards in case of decrease. At time 500 the dartboard is shifted only along ordinate. In case of a change in both, expectation and variance, the process leaves the circle in both horizontal and vertical direction. Indeed, at time 750, the dartboard is shifted south-west as there is a decline in both expectation and variance. Vice versa, the location of a dartboard facilitates change point interpretation, see Section 6.

### 3 The Model

**Notation** A sequence  $\mathbf{X} = (X_i)_{i=1,2,\dots}$  of i.i.d. real-valued RVs with  $\mathbb{E}[|X_1|^4] < \infty$  and positive variance  $\sigma^2 := \mathbb{V}\text{ar}(X_1) > 0$  is called an auxiliary process. We abbreviate the  $k$ -th moment  $\mu^{(k)} := \mathbb{E}[X_1^k]$  and the  $k$ -th centered moment  $\mu^{\{k\}} := \mathbb{E}[(X_1 - \mathbb{E}[X_1])^k]$  for  $k = 1, \dots, 4$ , the expectation  $\mu := \mu^{(1)}$ , and  $\nu^2 := \mathbb{V}\text{ar}((X_1 - \mu)^2) = \mu^{\{4\}} - \sigma^4$ , while  $\sigma^2 > 0$  implies  $\nu^2 > 0$ . We set  $\rho := \mu^{\{3\}}/(\sigma\nu)$  which is the correlation between  $X_1$  and  $(X_1 - \mu)^2$  as  $\text{Cov}(X_1, (X_1 - \mu)^2) = \text{Cov}(X_1 - \mu, (X_1 - \mu)^2) = \mu^{\{3\}}$ . It is  $|\rho| < 1$  as  $(X_1 - \mu)^2$  is not linear in  $X_1$ . Call  $\mu, \sigma^2, \nu^2, \rho, \mu^{\{k\}}$  and  $\mu^{(k)}$  the population parameters. For  $d = 1, 2, \dots$  let  $N_d(w, \Sigma)$  denote the  $d$ -variate normal distribution with expectation  $w \in \mathbb{R}^d$  and  $d \times d$  covariance matrix  $\Sigma$ . We mention joint asymptotic normality of the mean  $\hat{\mu} := (1/n) \sum_{i=1}^n X_i$  and the empirical variance  $\hat{\sigma}^2 := (1/n) \sum_{i=1}^n (X_i - \hat{\mu})^2$ , for  $n \rightarrow \infty$

$$\sqrt{n} \left[ \begin{pmatrix} \hat{\mu} \\ \hat{\sigma}^2 \end{pmatrix} - \begin{pmatrix} \mu \\ \sigma^2 \end{pmatrix} \right] \xrightarrow{d} N_2(0, \Sigma) \quad \text{with} \quad \Sigma := \begin{pmatrix} \sigma^2 & \rho\sigma\nu \\ \rho\sigma\nu & \nu^2 \end{pmatrix}, \quad (1)$$

while  $\xrightarrow{d}$  denotes convergence in distribution. For that rewrite  $\hat{\sigma}^2 = \hat{\mu}^{(2)} - \hat{\mu}^2$  using  $\hat{\mu}^{(2)} := (1/n) \sum_{i=1}^n X_i^2$ , and then apply the  $\delta$ -method w.r.t. the pair  $(\hat{\mu}, \hat{\mu}^{(2)})$ , the latter of which the bivariate central limit theorem holds true, see e.g., van der Vaart (1998) for details.  $\Sigma$  is regular as  $\det(\Sigma) = (1 - \rho)\sigma^2\nu^2 > 0$ . We study statistics in function space. For an interval  $[a, b] \subset \mathbb{R}_0$  let  $(\mathcal{D}_{\mathbb{R}^d}[a, b], d_{SK})$  and  $(\mathcal{D}_{\mathbb{R}^d}[a, b], \|\cdot\|)$  denote the spaces of  $\mathbb{R}^d$ -valued càdlàg-functions on  $[a, b]$  equipped with Skorokhod topology  $d_{SK}$  or the supremum norm  $\|\cdot\|$ . Convergence w.r.t.  $\|\cdot\|$  implies convergence regarding  $d_{SK}$ .

**The Model  $\mathcal{M}$**  A piecewise combination of auxiliary processes constitutes a process with change points: we fix  $T \in \mathbb{N} \setminus \{0, 1\}$  and call  $\{1, \dots, T\}$  the observation regime. Then we consider a subset  $C \subset \{1, \dots, T-1\}$  of cardinality  $m$  with ordered elements  $c_1 < c_2 < \dots < c_m$ . We call  $c_u$  the  $u$ -th change point and  $C$  the set of change points.  $C$  is treated fixed but unknown. Given  $C$  we consider  $m+1$  independent auxiliary processes  $\mathbf{X}_1, \dots, \mathbf{X}_{m+1}$ , with  $\mathbf{X}_u = (X_{u,i})_{i=1,2,\dots}$  having expectations  $\mu_u := \mathbb{E}[X_{u,1}]$  and variances  $\sigma_u^2 := \mathbb{V}\text{ar}(X_{u,1})$ , for  $u = 1, \dots, m+1$ . We assume

$$(\mu_u, \sigma_u^2) \neq (\mu_{u+1}, \sigma_{u+1}^2), \quad (2)$$

for  $u = 1, \dots, m$ , i.e., at any  $c_u$  either the expectation or the variance (or both) change, while other parameters are allowed to change as well. Then, a compound process is given by

$$X_{1,1}, \dots, X_{1,c_1}, X_{2,c_1+1}, \dots, X_{2,c_2}, \dots, X_{m+1,c_m+1}, \dots, X_{m+1,T}, \quad (3)$$

i.e., after change point  $c_u$ , we enter the process  $\mathbf{X}_{u+1}$  with the pair  $(\mu_{u+1}, \sigma_{u+1}^2)$ . Given  $T$ , the set  $\mathcal{M}$  of processes constructed in this fashion constitutes the model, see Figure 2 (and

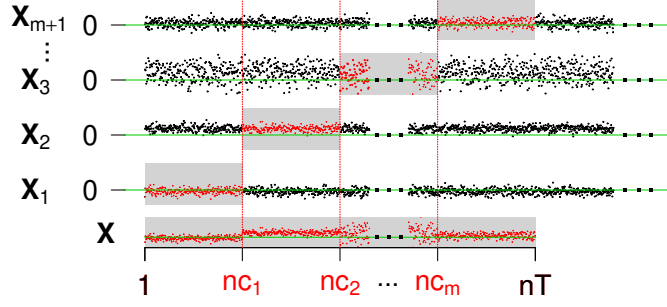


Figure 2: Construction of  $\mathbf{X} \in \mathcal{M}$  with  $m$  change points in the setup of general  $n$ .

set  $n=1$ ). For  $\mathbf{X} \in \mathcal{M}$  we aim at testing the null hypothesis  $C = \emptyset$ . In case of rejection we aim at estimating  $C$ . For a model  $\mathcal{M}$  we further introduce a window size

$$h \in \{2, 3, \dots, \lfloor T/2 \rfloor\}, \quad (4)$$

while  $\lfloor \cdot \rfloor$  denotes the floor function. The window size is  $h$  used to restrict the observation regime for local evaluation of  $\mathbf{X}$ . We often assume a minimal distance of  $2h$  between adjacent change points. A process  $\mathbf{X}$  with  $C = \emptyset$  derives from a single auxiliary process  $\mathbf{X}_1$  in which case we often set  $\mu := \mu_1$ ,  $\sigma^2 := \sigma_1^2$ ,  $\nu^2 := \nu_1^2$  etc.

Methodology is based on asymptotics for which we extend the model  $\mathcal{M}$  by letting  $T$ ,  $c_1, \dots, c_m$  and  $h$  to depend linearly on a parameter  $n$ , i.e., we switch to  $nT$ ,  $nc_1, \dots, nc_m$  and  $nh$ , for  $n \in \mathbb{N}$ . The extension from (3) then writes

$$X_{1,1}, \dots, X_{1,nc_1}, X_{2,nc_1+1}, \dots, X_{2,nc_2}, \dots, X_{m+1,nc_m+1}, \dots, X_{m+1,nT},$$

see Figure 2. Throughout we study asymptotics by letting  $n \rightarrow \infty$ . Increasing  $n$  means that we stay in each auxiliary process  $\mathbf{X}_u$  for a longer period, technically resulting in a triangular setup. The case  $n = 1$  is called the real time scenario. The dependence of  $\mathcal{M}$  and  $\mathbf{X}$  on  $n$  is suppressed for simplicity.

## 4 The moving sum processes

For  $\mathbf{X} \in \mathcal{M}$  we study two moving sum processes as there are two types of changes involved, changes in the expectation and changes in the variance. The idea is to locally evaluate the RVs restricted to a *left* window  $(t-h, t]$  and an adjacent *right* window  $(t, t+h]$ . A comparison of means is sensitive to changes in the expectation and a comparison of empirical variances is sensitive to changes in the variance.

**Definition of  $(E_{h,t}^{(n)})_t$  and  $(V_{h,t}^{(n)})_t$  via local parameter estimators** Let  $h$  be a window size as in (4) and  $t \in [h, T-h]$ . For  $n = 1, 2, \dots$  set

$$E_{h,t}^{(n)} := \frac{\hat{\mu}_r - \hat{\mu}_\ell}{[(\hat{\sigma}_r^2 + \hat{\sigma}_\ell^2)/(nh)]^{1/2}} \quad \text{and} \quad V_{h,t}^{(n)} := \frac{\hat{\sigma}_r^2 - \hat{\sigma}_\ell^2}{[(\hat{\nu}_r^2 + \hat{\nu}_\ell^2)/(nh)]^{1/2}}. \quad (5)$$

We state the estimators in (5). The subscripts  $\ell$  and  $r$  indicate a local evaluation of  $\mathbf{X} = (X_i)_{i=1, \dots, nT}$ . For that let

$$I_\ell := \{\lfloor n(t-h) \rfloor + 1, \dots, \lfloor nt \rfloor\} \quad \text{and} \quad I_r := \{\lfloor nt \rfloor + 1, \dots, \lfloor n(t+h) \rfloor\} \quad (6)$$

denote the indices associated with the left and the right window, see Figure 3. The sets  $I_\ell$  and  $I_r$  depend on  $n, t$  and  $h$  which is inherited to the statistics introduced in the following, but suppressed to avoid notational overload. We restrict  $\mathbf{X}$  to the  $nh$  RVs related to  $I_j$ : for

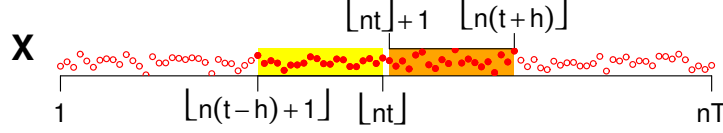


Figure 3: Schematic representation of  $I_\ell$  and  $I_r$ . The marginals of  $\mathbf{X}$  that refer to  $I_\ell$  are accentuated by the yellow box and those of  $I_r$  by the orange box.

$j \in \{\ell, r\}$  and  $k \in \{1, \dots, 4\}$  we define local, time dependent estimators for the  $k$ -th moment  $\mu^{(k)}$  and centered moment  $\mu^{\{k\}}$  via their empirical analogies

$$\hat{\mu}_j^{(k)} := \frac{1}{nh} \sum_{i \in I_j} X_i^k \quad \text{and} \quad \hat{\mu}_j^{\{k\}} := \frac{1}{nh} \sum_{i \in I_j} (X_i - \hat{\mu}_j^{(1)})^k, \quad (7)$$

which yield local estimators for the population parameters  $\mu, \sigma^2$  and  $\nu^2$  via

$$\hat{\mu}_j := \hat{\mu}_j^{(1)}, \quad \hat{\sigma}_j^2 := \hat{\mu}_j^{\{2\}} \quad \text{and} \quad \hat{\nu}_j^2 := \hat{\mu}_j^{\{4\}} - \hat{\sigma}_j^4, \quad (8)$$

while the notion of *the* population parameter is only well-defined if  $C = \emptyset$ . The local aspect of the estimators is inherited to  $E_{h,t}^{(n)}$  and  $V_{h,t}^{(n)}$ . If we omit the superscript  $n$  of a statistic this abbreviates  $n = 1$ , e.g.,  $E_{h,t} := E_{h,t}^{(1)}$ .

We study stochastic processes. For  $n = 1, 2, \dots$  the estimators in (7) and (8) and thus  $(E_{h,t}^{(n)})_t$  and  $(V_{h,t}^{(n)})_t$  constitute processes in  $(\mathcal{D}_{\mathbb{R}}[h, T-h], d_{SK})$  with step-paths and discontinuities limited to the set  $\{h + k/n \mid k = 1, 2, \dots, n(T-2h)\}$ . Continuity from right results from the floor function in (6). See Figure 1 for  $(E_{h,t})_t$  (B, magenta) and  $(V_{h,t})_t$  (C, blue) evaluated from the process  $\mathbf{X}$  (A, red). In the absence of change points the estimators are functionally strongly consistent for their population parameters:

**Lemma 4.1.** *Let  $\mathbf{X} \in \mathcal{M}$  with  $C = \emptyset$ . For  $j \in \{\ell, r\}$  it holds in  $(\mathcal{D}_{\mathbb{R}}[h, T-h], d_{\|\cdot\|})$  as  $n \rightarrow \infty$  almost surely that  $(\hat{\mu}_j^{(k)})_t \rightarrow (\mu^{(k)})_t$  for  $k \in \{1, \dots, 4\}$ ,  $(\hat{\sigma}_j^2)_t \rightarrow (\sigma^2)_t$  and  $(\hat{\nu}_j^2)_t \rightarrow (\nu^2)_t$ .*

The proof relies on a functional strong law of large numbers.

**The joint process  $(J_{h,t}^{(n)})_t$**  The crucial object of study is the joint process  $(J_{h,t}^{(n)})_t$  given as  $J_{h,t}^{(n)} := (E_{h,t}^{(n)}, V_{h,t}^{(n)})^t$ , see Figure 1D. We consider  $(J_{h,t}^{(n)})_t$  in function space  $(\mathcal{D}_{\mathbb{R}^2}[h, T-h], d_{SK})$ . Weak convergence to a bivariate Gaussian process is shown first under  $C = \emptyset$ , see Proposition 4.2. This is used for the construction of the statistical test in Section 5. Second, convergences are also shown in case of  $C \neq \emptyset$ , see Proposition 7.1 and Lemma 6.2, which support the change point detection algorithm developed in Section 6. Gaussian limits seem reasonable as the asymptotic normality in (1) inherits to  $E_{h,t}^{(n)}$  and  $V_{h,t}^{(n)}$  and thus to  $J_{h,t}^{(n)}$ .

In the remainder of this section we study the asymptotics of  $(J_{h,t}^{(n)})_t$  under  $C = \emptyset$ . Both components of  $(J_{h,t}^{(n)})_t$  are evaluated from the same process  $\mathbf{X}$  and thus found correlated in general. In Figure 4A we see that  $(J_{h,t})_t$  has a preferred direction of variability along the diagonal  $x = y$ . Symmetry  $\mu^{\{3\}} = 0$  of the RVs is necessary and sufficient for the components to be asymptotically independent. Vice versa skewness  $\mu^{\{3\}} \neq 0$  results in correlated components. Skewness is captured in a correlation matrix  $\Gamma$ .

**Proposition 4.2.** *Let  $\mathbf{X} \in \mathcal{M}$  with  $C = \emptyset$ . In  $(\mathcal{D}_{\mathbb{R}^2}[h, T-h], d_{SK})$*

$$(\Gamma^{-1/2} \cdot J_{h,t}^{(n)})_t \xrightarrow{d} (\mathcal{L}_{h,t})_t,$$

as  $n \rightarrow \infty$ , with  $\Gamma^{-1/2}$  in (11) and  $(\mathcal{L}_{h,t})_t$  in (9).

The proof is based on the bivariate functional central limit theorem w.r.t. the two components  $X_i$  and  $(X_i - \mu)^2$  ( $\leftrightarrow$  mean and variance). We state  $(\mathcal{L}_{h,t})_t$  and  $\Gamma^{-1/2}$ . The bivariate limit process  $(\mathcal{L}_{h,t})_t$  is given via

$$\mathcal{L}_{h,t} := \left( \frac{(W_{t+h} - W_t) - (W_t - W_{t-h})}{\sqrt{2h}}, \frac{(\mathcal{W}_{t+h} - \mathcal{W}_t) - (\mathcal{W}_t - \mathcal{W}_{t-h})}{\sqrt{2h}} \right)^t, \quad (9)$$

while  $(W, \mathcal{W}) := (W_t, \mathcal{W}_t)_{t \geq 0}$  denotes a planar Brownian motion. The intrinsic structure of the double windows is preserved.  $(\mathcal{L}_{h,t})_t$  is a continuous  $2h$ -dependent bivariate Gaussian process. It is isotropic and its components have zero mean and unit variance. Isotropy inherits from  $(W, \mathcal{W})$ . For all  $t \in [h, T-h]$  we find  $\mathcal{L}_{h,t} \sim N_2(0, I)$ , while  $I$  denotes the identity matrix.

$\Gamma^{-1/2}$  is a  $2 \times 2$  matrix that corrects  $(J_{h,t}^{(n)})_t$  for its preferred direction of variability. Recall  $\rho = \mu^{\{3\}}/(\sigma\nu)$ , which is captured in the correlation matrix

$$\Gamma := \text{Corr} \begin{pmatrix} X_1 \\ (X_1 - \mu)^2 \end{pmatrix} = \begin{pmatrix} 1 & \rho \\ \rho & 1 \end{pmatrix}. \quad (10)$$

$\Gamma$  is regular as  $|\rho| < 1$ , see Section 3. A root  $\Gamma^{1/2}$  and its inverse  $\Gamma^{-1/2}$  is obtained by solving the eigenvalue problem regarding  $\Gamma$ . We first decompose

$$\Gamma = ADA^t := \begin{pmatrix} 1/\sqrt{2} & 1/\sqrt{2} \\ 1/\sqrt{2} & -1/\sqrt{2} \end{pmatrix} \cdot \begin{pmatrix} 1+\rho & 0 \\ 0 & 1-\rho \end{pmatrix} \cdot \begin{pmatrix} 1/\sqrt{2} & 1/\sqrt{2} \\ 1/\sqrt{2} & -1/\sqrt{2} \end{pmatrix}.$$

The matrix  $A$  is orthogonal and interpreted a change of basis. Since  $\Gamma$  is a correlation (not only covariance) matrix, the columns of  $A$  do not depend on  $\rho$  but always span the diagonals  $x = y$  and  $x = -y$ . A root or inverse root of  $\Gamma$  is obtained by replacing the diagonal elements of  $D$  with their roots  $\sqrt{1 \pm \rho}$  or their roots' reciprocals  $1/\sqrt{1 \pm \rho}$ , yielding

$$\begin{aligned} \Gamma^{1/2} &= \frac{1}{2} \begin{pmatrix} \sqrt{1+\rho} + \sqrt{1-\rho} & \sqrt{1+\rho} - \sqrt{1-\rho} \\ \sqrt{1+\rho} - \sqrt{1-\rho} & \sqrt{1+\rho} + \sqrt{1-\rho} \end{pmatrix} \quad \text{and} \\ \Gamma^{-1/2} &= \frac{1}{2} \begin{pmatrix} (1/\sqrt{1+\rho}) + (1/\sqrt{1-\rho}) & (1/\sqrt{1+\rho}) - (1/\sqrt{1-\rho}) \\ (1/\sqrt{1+\rho}) - (1/\sqrt{1-\rho}) & (1/\sqrt{1+\rho}) + (1/\sqrt{1-\rho}) \end{pmatrix}. \end{aligned} \quad (11)$$

Symmetry  $\rho = 0$  means  $\Gamma = I = \Gamma^{1/2} = \Gamma^{-1/2}$ . For an example of a skewed distribution consider  $\text{gamma}(p, \lambda)$  with parameters shape  $p > 0$  and rate  $\lambda > 0$ , see also Figure 4A. We obtain  $\sigma^2 = p/\lambda^2$ ,  $\nu^2 = 2[p^2 + 3p]/\lambda^4$  and  $\mu^{\{3\}} = 2p/\lambda^3$ , and  $\rho = (2/[p+3])^{1/2} > 0$  depending only on  $p$ .

## 5 The statistical test

We derive the test for the null hypothesis  $C = \emptyset$ . We use the joint convergence of  $(J_{h,t}^{(n)})_t$  from Proposition 4.2 and derive a rejection boundary from the limit process  $(\mathcal{L}_{h,t})_t$  in Monte



Carlo simulations. We differentiate two cases: first, symmetric RVs result in the asymptotic isotropy of  $(J_{h,t}^{(n)})_t$  and we choose the boundary a circle, see Figure 1. Second, in the general case of possibly skewed RVs we choose the boundary an ellipse or a square, see Figure 4. This is due to  $(J_{h,t}^{(n)})_t$  generally having a preferred direction of variability along  $x = y$  or  $x = -y$ .

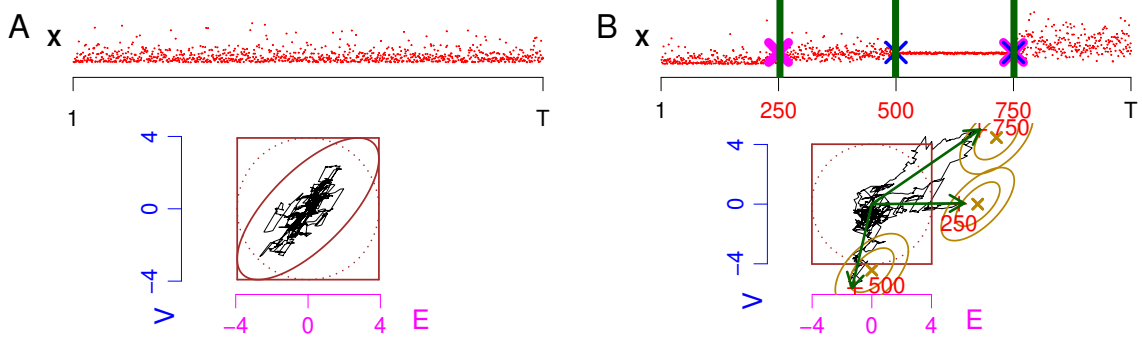


Figure 4: The bivariate procedure for skewed RVs. Upper segment: process  $\mathbf{X} \in \mathcal{M}$ . Lower segment:  $(J_{h,t})_t$  (black), rejection boundaries (brown) either via ellipse  $\mathcal{E}$  or square  $\mathcal{S}$  ( $\supset \mathcal{E}$ ) derive from dotted circle  $\mathcal{C}$ . A:  $C = \emptyset$ ,  $\exp(1)$  distribution,  $(J_{h,t})_t$  does not leave  $\mathcal{E}$  (and thus not  $\mathcal{S}$ ), hence no rejection of  $C = \emptyset$ . B: Three change points  $C = \{250, 500, 750\}$ , gamma distribution, expectations 0.8, 2, 2, 4, standard deviations 1, 1, 0.1, 2. Rejection of  $C = \emptyset$  as  $(J_{h,t})_t$  leaves  $\mathcal{S}$ . Three change points  $\hat{C} = \{253, 499, 751\}$  (green bars) detected. Red crosses (+) mark  $J_{h,c}$  for  $c \in C$ . Golden ellipses mark the 66%- and 95%-contour lines of the asymptotic distribution of  $J_{h,c}^{(n)}$ . Skewness results in squeezed dartboards. Increase in expectation at 250 shifts the dartboard right, decrease in variance at 500 shifts it downwards, and increase in both expectation and variance at time 750 shifts it north-east.

**Derivation of the test** Let  $C = \emptyset$ . Proposition 4.2 states that  $(\Gamma^{-1/2} \cdot J_{h,t}^{(n)})_t$  asymptotically fluctuates around zero with no direction preferred. Thus, a large deviation of  $\Gamma^{-1/2} \cdot J_{h,t}^{(n)}$  from zero for some  $t$  indicates a violation from the null hypothesis. To measure this deviation we mention the equality  $d_I(\Gamma^{-1/2} \cdot J_{h,t}^{(n)}) = d_\Gamma(J_{h,t}^{(n)})$ , while  $d_I((x, y)^t) = (x^2 + y^2)^{1/2}$  denotes the Euclidean and  $d_\Gamma((x, y)^t) = [(x, y) \cdot \Gamma^{-1} \cdot (x, y)^t]^{1/2}$  the Mahalanobis distance, for  $(x, y)^t \in \mathbb{R}^2$ . Proposition 4.2 and continuous mapping imply convergence of the maximal Mahalanobis distance, as  $n \rightarrow \infty$

$$M_h^{(n)}(\Gamma) := \max_{t \in [h, T-h]} d_\Gamma(J_{h,t}^{(n)}) \xrightarrow{d} \max_{t \in [h, T-h]} d_I(\mathcal{L}_{h,t}). \quad (12)$$

We use  $M_h(\Gamma) := M_h^{(1)}(\Gamma)$  as a test statistic. We reject iff  $M_h(\Gamma)$  exceeds some value  $Q$ . For an asymptotic significance level  $\alpha \in (0, 1)$ , the value of  $Q$  should be chosen the  $(1 - \alpha)$ -quantile of the limit distribution in (12). To the best of our knowledge there is no closed formula available. To approximate a quantile we could aim at deriving tail bounds, see e.g., Albin (1990); Lindgren (1980); Adler (1990); Talagrand (2014) mentioning that  $[d_I^2(\mathcal{L}_{h,t})]_t$  constitutes a  $\chi^2$ -process. However, it is more accurate to choose  $Q$  a quantile of the approximated distribution derived in Monte Carlo simulations.

Equivalently, instead of comparing the maximal distance  $M_h(\Gamma)$  to  $Q \in \mathbb{R}$ , we can judge the entire process  $(J_{h,t})_t$  w.r.t. to a rejection area  $\mathcal{R} \subset \mathbb{R}^2$ . For that we define the ellipse  $\mathcal{E} := \{(x, y)^t \in \mathbb{R}^2 \mid d_\Gamma((x, y)^t) \leq Q\}$ , see Figure 4A. The null hypothesis is rejected iff

$(J_{h,t})_t$  enters  $\mathcal{R} = \mathcal{E}^c$  at any time, while the superscript  $c$  indicates the complement in  $\mathbb{R}^2$ . In case of symmetry  $\Gamma = I$ , the ellipse equals a circle  $\mathcal{C}$  with radius  $Q$ , i.e.,  $\mathcal{C} := \{(x, y)^t \in \mathbb{R}^2 \mid d_I((x, y)^t) \leq Q\}$ , thus  $\mathcal{R} = \mathcal{C}^c$ , see Figure 1. For skewed RVs the ellipse derives from the circle by squeezing,  $\mathcal{E} = \Gamma^{1/2} \cdot \mathcal{C} = \{\Gamma^{1/2} \cdot (x, y)^t \mid (x, y)^t \in \mathcal{C}\}$ . Note that if  $C \neq \emptyset$  there is no concept of a single ellipse as  $\Gamma$  generally varies between change points.

**Treatment of the unknown correlation  $\rho$**  The statistic  $M_h(\Gamma)$  is not yet practically applicable as  $\Gamma$  depends on  $\rho = \mu^{\{3\}}/(\sigma\nu)$  unknown. We discuss three ways to cope with  $\rho$ . First, the additional assumption of symmetry  $\rho = 0$  yields  $M_h(I)$ . Second, we consistently estimate  $\rho$  locally by

$$\hat{\rho} := \frac{\hat{\mu}_r^{\{3\}} + \hat{\mu}_\ell^{\{3\}}}{(\hat{\sigma}_r^2 + \hat{\sigma}_\ell^2)^{1/2} \cdot (\hat{\nu}_r^2 + \hat{\nu}_\ell^2)^{1/2}}, \quad (13)$$

with estimators in (7) and (8). The dependence of  $\hat{\rho}$  on  $n$ ,  $t$  and  $h$  is suppressed. Lemma (4.1) implies that in  $(D_{\mathbb{R}}[h, T-h], d_{SK})$  it holds  $(\hat{\rho})_t \rightarrow (\rho)_t$  a.s., if  $C = \emptyset$ . Define local time dependent estimators  $\hat{\Gamma}$ ,  $\hat{\Gamma}^{1/2}$  and  $\hat{\Gamma}^{-1/2}$  by replacing  $\rho$  by  $\hat{\rho}$  in (10) and (11). Then Slutsky's Lemma implies Proposition 4.2 to hold true for  $\Gamma^{1/2}$  replaced by  $\hat{\Gamma}^{1/2}$ . The test statistic from (12) writes

$$M_h(\hat{\Gamma}) := \max_t d_{\hat{\Gamma}}(J_{h,t}). \quad (14)$$

Thinking in terms of the joint process  $(J_{h,t})_t$ , the rejection ellipse  $\hat{\mathcal{E}} := \hat{\Gamma}^{1/2} \cdot \mathcal{C}$  becomes time dependent due to the estimation  $\hat{\Gamma}$ . If  $C = \emptyset$ , estimation is consistent and the asymptotic significance level is kept at  $\alpha$ .

The third approach to tackle  $\rho$  is to neglect both the circle  $\mathcal{C}$  as well as the ellipse  $\mathcal{E} = \Gamma^{1/2} \cdot \mathcal{C}$  and to use the square  $\mathcal{S} := \{(x, y)^t \in \mathbb{R}^2 \mid d_\infty((x, y)^t) \leq Q\}$  instead, while  $d_\infty((x, y)^t) := \max(|x|, |y|)$  denotes the maximum norm. The square has center zero and an edge length equal to the diameter of  $\mathcal{C}$ . As  $\Gamma$  has unit diagonals any ellipse  $\mathcal{E}$  is trapped in the square  $\mathcal{S} \supset \mathcal{E}$ , see Figure 4A. Thus, a conservative approach to avoid estimation is the choice  $\mathcal{R} := \mathcal{S}^c$ , such that the asymptotic probability to falsely reject the null hypothesis is less than  $\alpha$ . The test statistic writes as

$$M_h(\infty) := \max_t d_\infty(J_{h,t}). \quad (15)$$

This approach is optimal in the sense that the ellipse  $\mathcal{E}$  touches each edge of the square  $\mathcal{S}$  exactly once and thus the square can not be shrunk further. In summary we differentiate three options for practice, see table 1.

test statistic	asympt. level	rejection area $\mathcal{R}$ w.r.t. $(J_{h,t})_t$	assumption
$M_h(I)$ (12)	$= \alpha$	$\mathcal{C}^c = \{(x, y)^t \in \mathbb{R}^2 \mid d_I((x, y)^t) > Q\}$	symmetry
$M_h(\hat{\Gamma})$ (14)	$= \alpha$	$\hat{\mathcal{E}}^c = \hat{\Gamma} \cdot \mathcal{C}^c$ , time dependent	/
$M_h(\infty)$ (15)	$< \alpha$	$\mathcal{S}^c = \{(x, y)^t \in \mathbb{R}^2 \mid d_\infty((x, y)^t) > Q\}$	/

Table 1: Three ways of testing.

Note that the bivariate nature of the test avoids double testing as compared to the two univariate approaches discussed in Section 2. Investigating  $(E_{h,t})_t$  and  $(V_{h,t})_t$  separately we

can simulate a quantile of the temporal maximum of a single component of  $(\mathcal{L}_{h,t})_t$ . Set  $\alpha = 5\%$ . In the univariate approaches we obtain the boundaries  $\approx \pm 3.59$ , see Figure 1 segments B and C. For the bivariate procedure we obtain  $Q \approx 4.00$  (radius in segment D), and this slight increase is the price for the avoidance of  $\alpha$ -error accumulation.

## 6 Change point detection

After rejection of the null hypothesis  $C = \emptyset$  we detect change points via successive arg max estimation, see Figure 5. We describe the estimation procedure. Then we state the asymptotic distribution of  $J_{h,c}^{(n)}$  at a change point  $c$  in Lemma 6.2, which describes the golden dartboards in Figures 1 and 4. The result is used to infer on the effects, i.e., the strength and the type of the change, which again is used for change point interpretation in practice.

**Algorithm 6.1.** Set  $\mathcal{R}$  as either  $\mathcal{C}^c$ ,  $\mathcal{E}^c$  or  $\mathcal{S}^c$  as used in the test. Set  $\hat{C}_h := \emptyset$  and  $\tau_h := [h, T - h] \cap \mathbb{N}$ . While  $J_{h,t} \in \mathcal{R}$  for any  $t \in \tau_h$ , update  $\hat{C}_h$  and  $\tau_h$  as follows: among all  $t \in \tau_h$  for which  $J_{h,t} \in \mathcal{R}$ , choose the candidate  $\hat{c}$  that maximizes the Euclidean distance of  $J_{h,t}$ , add  $\hat{c}$  to  $\hat{C}_h$  and delete its  $h$ -neighborhood  $\{\hat{c} - h + 1, \dots, \hat{c} + h\}$  from  $\tau_h$ .

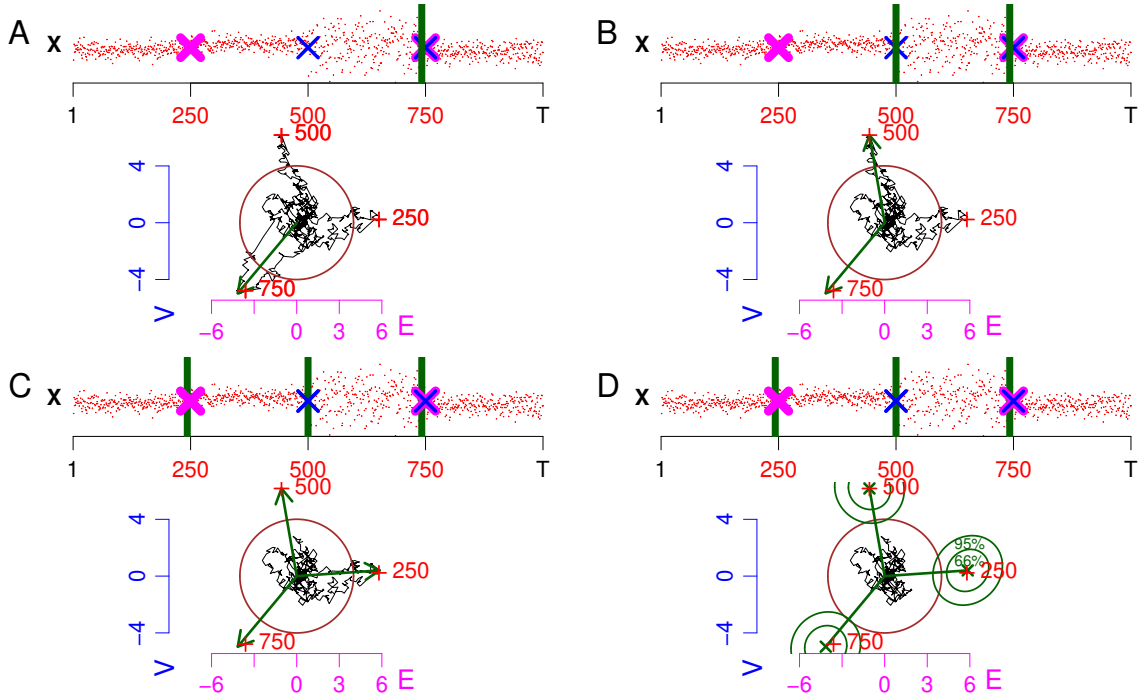


Figure 5: Change point detection via successive arg max estimation, setup from Figure 1II. A,B,C: Obtain new estimate  $\hat{c}$  (green bar) as the integer that satisfies  $J_{h,\hat{c}} = \max_t d_I(J_{h,t})$  (green arrow). Cut out  $(J_{h,t})_t$  in the  $h$ -neighborhood of  $\hat{c}$  (B,C,D). D: Stop as remaining  $(J_{h,t})_t$  lies in  $\mathcal{R} = \mathcal{C}$  (brown circle). Estimated distribution of  $J_{h,\hat{c}}$  shown via 66%- and 95%-contour lines (green dartboards).

Note that for any choice of  $\mathcal{R}$ , either  $\mathcal{C}^c$ ,  $\mathcal{E}^c$  or  $\mathcal{S}^c$ , it is always the Euclidean distance that inference is based on, see interpretation below.

**Asymptotic normality of  $J_{h,c}^{(n)}$**

**Lemma 6.2.** *Let  $\mathbf{X} \in \mathcal{M}$ ,  $h$  a window size, and  $c \in [h, T - h]$  a change point such that  $(c - h, c + h] \setminus \{c\}$  is free from change points. Then*

$$J_{h,c}^{(n)} - \Delta_{h,c}^{(n)} \cdot j_{h,c}^{(n)} \xrightarrow{d} N_2(0, \Gamma_c),$$

as  $n \rightarrow \infty$ , with  $\Delta_{h,c}^{(n)}$  and  $j_{h,c}^{(n)}$  in (16) and  $\Gamma_c$  in (17).

The proof is based on the multivariate  $\delta$ -method which connects the population left and right of  $c$ . We state  $\Delta_{h,c}^{(n)}$ ,  $j_{h,c}^{(n)}$  and  $\Gamma_c$ . Consider the first change point  $c := c_1$ . Left and right from  $c$  the process  $\mathbf{X}$  derives from the two auxiliary processes  $\mathbf{X}_u = (X_{u,i})_{i=1,2,\dots}$  for  $u \in \{1, 2\}$ , with population parameters  $\mu_u$ ,  $\sigma_u^2$ ,  $\nu_u^2$  and  $\mu_u^{\{3\}}$ . We set

$$j_{h,c}^{(n)} := \begin{pmatrix} \frac{\mu_2 - \mu_1}{[(\sigma_2^2 + \sigma_1^2)/(nh)]^{1/2}} \\ \frac{\sigma_2^2 - \sigma_1^2}{[(\nu_2^2 + \nu_1^2)/(nh)]^{1/2}} \end{pmatrix} \quad \text{and} \quad \Delta_{h,c}^{(n)} := \begin{pmatrix} \left(\frac{\sigma_2^2 + \sigma_1^2}{\hat{\sigma}_r^2 + \hat{\sigma}_\ell^2}\right)^{1/2} & 0 \\ 0 & \left(\frac{\nu_2^2 + \nu_1^2}{\hat{\nu}_r^2 + \hat{\nu}_\ell^2}\right)^{1/2} \end{pmatrix}, \quad (16)$$

and call  $j_{h,c}^{(n)}$  the asymptotic expectation of  $J_{h,c}^{(n)}$ . The  $2 \times 2$  diagonal matrix  $\Delta_{h,c}^{(n)}$  replaces the true order of scaling of the components of  $J_{h,c}^{(n)}$  with the local estimators. Lemma 4.1 implies  $\Delta_{h,c}^{(n)} \rightarrow I$  a.s. componentwise as  $n \rightarrow \infty$ . The asymptotic correlation matrix is given by

$$\Gamma_c := \begin{pmatrix} 1 & \rho_c \\ \rho_c & 1 \end{pmatrix} \quad \text{with} \quad \rho_c := \frac{\mu_2^{\{3\}} + \mu_1^{\{3\}}}{(\sigma_2^2 + \sigma_1^2)^{1/2} \cdot (\nu_2^2 + \nu_1^2)^{1/2}}. \quad (17)$$

Note that  $\rho_c$  has the same structure as its estimator  $\hat{\rho}$  in (13). For the  $u$ -th change point replace in (16) and (17) the indices 1 and 2 with  $u$  and  $u + 1$ . In Figures 1 and 4 the distribution of  $J_{h,c}$  is approximated by the  $N_2(j_{h,c}^{(1)}, \Gamma_c)$  distribution for the three change points. The golden dartboards describe the 66%- and 95%-contour lines with center  $j_{h,c}^{(1)}$ . The larger the absolute correlation  $|\rho_c|$ , the more squeezed we find the dartboards in Figure 4B. Symmetry implies  $\rho_c = 0$  such that the dartboards in Figure 1 are not at all squeezed. The magnitude of any dartboard is unique up to squeezing as  $\Gamma_c$  is a correlation matrix with unit diagonals. Indeed, bivariate normality implies that for  $\alpha \in (0, 1)$  any  $\alpha$ -contour ellipse is trapped optimally in a square with edge lengths  $2\sqrt{q_\alpha}$ , while  $q_\alpha$  denotes the  $\alpha$ -quantile of the  $\chi^2$ -distribution with two degrees of freedom. If  $\mu_1 = \mu_2$ ,  $\sigma_1^2 = \sigma_2^2$  and  $\rho_1 = \rho_2$  then Lemma 6.2 states  $J_{h,c}^{(n)} \xrightarrow{d} N_2(0, I)$  which aligns with Proposition 4.2.

**Change point interpretation** To interpret effects we decompose

$$j_{h,c}^{(n)} = \sqrt{nh} \cdot d_I(j_c) \cdot (\cos(\omega), \sin(\omega))^t$$

with  $j_c := j_{h,c}^{(n)}/\sqrt{nh}$  and  $\omega \in [0, 2\pi)$  the angle between  $j_c$  and the abscissa. We comment on the factors. First,  $\sqrt{nh}$  derives from the artificial parameter  $n$  and the choice of the window  $h$ . The larger they are chosen, the further the dartboard is pushed away from zero (as long as no other change point is overlapped). We interpret  $j_c$  a signal to noise ratio that captures the effects: the Euclidean distance  $d_I(j_c)$  is a measure for the strength of the change. The angle  $\omega$  is interpreted as the type of the change with special cases  $\omega \in \{0, \pi\} \Leftrightarrow$  change

only in expectation ( $0 = \text{increase}, \pi = \text{decrease}$ ), and  $\omega \in \{\pi/2, (3/2)\pi\} \Leftrightarrow$  change only in variance ( $\pi/2 = \text{increase}, (3/2)\pi = \text{decrease}$ ). Generally, a dartboard is shifted towards  $(\cos(\omega), \sin(\omega))^t$ , see Figure 1 or 4. We strengthen that a dartboard lies far off of zero if either the technical factor  $\sqrt{nh}$ , or the strength of the change, i.e., the Euclidean distance  $d_I(j_c)$ , is large. This result is universal in the sense that it is not a consequence of the presence or absence of symmetry of the underlying process  $\mathbf{X}$  – the aspect of symmetry is captured the correlation matrix  $\Gamma_c$ , but not in the expectation  $j_{h,c}^{(n)}$ . This is why in algorithm 6.1 it is always the Euclidean distance that the joint process is judged with, regardless of  $\mathcal{R}$ .

In practice, interpretation is based on the joint statistic  $J_{h,\hat{c}}$  at the time of an estimated change point  $\hat{c}$ , see green arrows in Figure 5. We assign the 66%- and 95%-contour lines of the  $N_2(J_{h,\hat{c}}, \hat{\Gamma}_{\hat{c}})$  distribution while  $\hat{\Gamma}_{\hat{c}}$  relies on the evaluation  $\hat{\rho}$  at time  $\hat{c}$  as in (13), see green dartboards in Figure 5D which are considered estimated counterparts of unknown golden dartboards. They are interpreted the error of  $J_{h,\hat{c}}$ , i.e., they strengthen confidence in change point interpretation: first, they give us an idea of how unlikely the detection of the change point was, if it was actually not at all present. The further the dartboard is shifted away from the rejection boundary, the harder it is to explain a false detection by chance. In other words, the green dartboards approximate the variability of the strength of the estimated change. Second, the green dartboards also approximate the variability of the type of the estimated change. For example in Figure 5D, the deviation of the right dartboard from the abscissa as well as the deviation of the upper dartboard from the ordinate can be easily explained by chance. It is not unlikely that the first estimate refers to change only in expectation and that the second estimate indicates a change only in variance. In contrast, for the dartboard in the lower left corner it is hard to argue that it refers to a change only in a single parameter. Due to the estimation  $\hat{\Gamma}_{\hat{c}}$  the dartboards are slightly squeezed despite of symmetry  $\Gamma_c = I$ .

## 7 The joint process in case of change points

Let  $\mathbf{X} \in \mathcal{M}$  with  $\rho_u = 0$  (symmetric RVs) and  $C \neq \emptyset$  with change points separated by at least  $2h$ . From Proposition 7.1 it will follow that approximately

$$(J_{h,t})_t \stackrel{d}{\approx} (j_{h,t})_t + (\mathcal{L}_{h,t}^*)_t,$$

with non-random centering  $(j_{h,t})_t$  which describes systematic deviations from zero which occur in the  $h$ -neighborhood of change points, and  $(\mathcal{L}_{h,t}^*)_t$  is a Gaussian process that fluctuates around zero. Figure 6 extends Figure 1 panels II and III. The centering terms around the three change points are colored in red, green and light blue, and the processes fluctuate close to them. In segment D we think of a golden dartboard that is traversing along systematic excursions. For the true change points the dartboards are depicted. The centering  $(j_{h,t})_t$  will explicitly state the sensitivity of  $(J_{h,t})_t$  to the effects: the first component is sensitive to changes in expectation and robustness against in higher order changes. The second component sensitivity to changes in the variance and robustness against higher order changes. This supports the performance of the change point detection algorithm. However,  $(j_{h,t})_t$  also reveals the error in the second component caused by a change in expectation, segment IIIC (red). In segment IIID (red) we see that this systematic error in inference is overcome in the bivariate procedure: for any excursion the centering takes its maximal Euclidean distance at the change point. To simplify notation we assume  $C = \{c\}$  but mention direct extensions to multiple change points separated by at least  $2h$ .

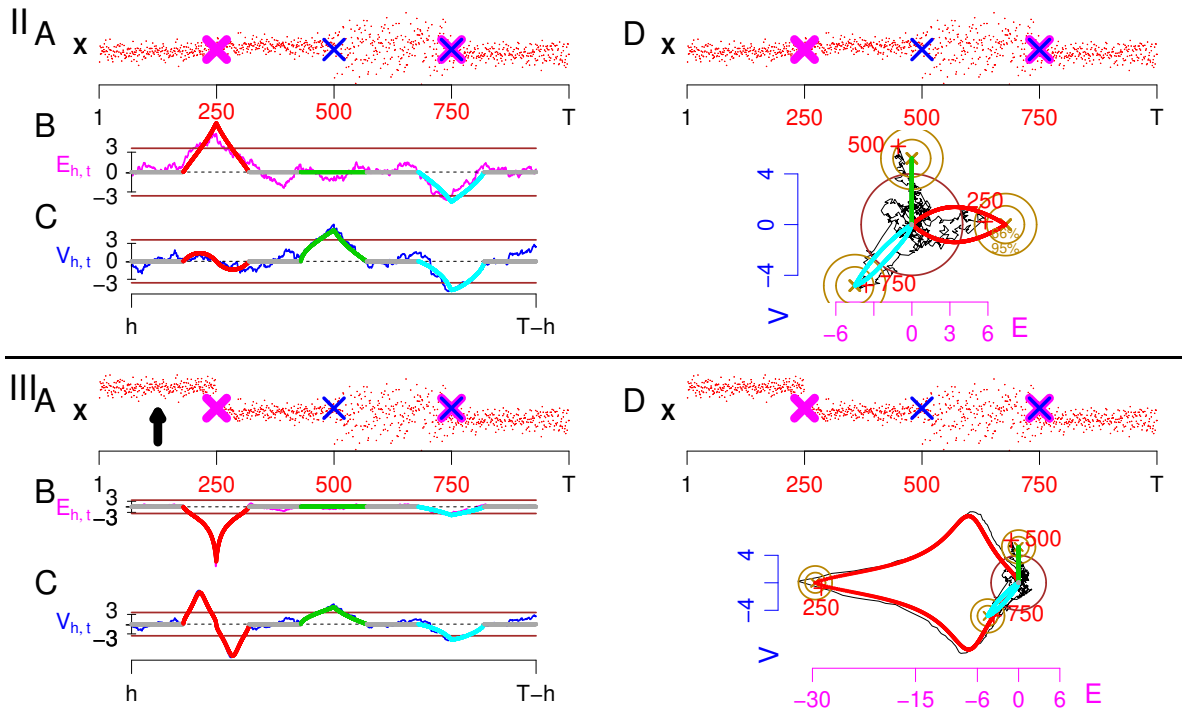


Figure 6: The centering terms  $(e_{h,t})_t$  (B),  $(v_{h,t})_t$  (C) and  $(j_{h,t})_t$  (D), colored inside the  $h$ -neighborhood of a change point (red around 250, green around 500, light blue around 750), else gray at zero. Extension of Figure 1 panels II and III.

**Proposition 7.1.** *Let  $\mathbf{X} \in \mathcal{M}$  with  $C = \{c\}$  and  $h$  a window size such that  $c \in [h, T - h]$ , and let  $\rho_1 = \rho_2 = 0$ . In  $(\mathcal{D}_{\mathbb{R}^2}[h, T - h], d_{SK})$*

$$\left[ \tilde{D}_{h,t} \cdot \left( J_{h,t}^{(n)} - \Delta_{h,t}^{(n)} \cdot j_{h,t}^{(n)} \right) \right]_t \xrightarrow{d} (\mathcal{L}_{h,t}^*)_t, \quad (18)$$

as  $n \rightarrow \infty$ , with  $(j_{h,t}^{(n)})_t$  in (21) and  $(\tilde{D}_{h,t})_t$ ,  $(\Delta_{h,t}^{(n)})_t$  in (22), and  $(\mathcal{L}_{h,t}^*)_t$  is a continuous  $2h$ -dependent bivariate process with  $\mathcal{L}_{h,t}^* \sim N_2(0, I)$  for all  $t$ .

This extends Proposition 4.2,  $(J_{h,t}^{(n)})_t \xrightarrow{d} (\mathcal{L}_{h,t})_t$  if  $C = \emptyset$ , and also the marginal result of Lemma 6.2,  $J_{h,c}^{(n)} - \Delta_{h,c}^{(n)} \cdot j_{h,c}^{(n)} \xrightarrow{d} N_2(0, I)$ . The proof jointly applies two bivariate functional central limit theorems to connect auxiliary processes left and right of  $c$ . In the following we explicitly state the quantities in (18). For that we first derive the asymptotics of the moments for  $C = \{c\}$ :

**Lemma 7.2.** *Let  $\mathbf{X} \in \mathcal{M}$  with  $C = \{c\}$  and  $h$  a window size such that  $c \in [h, T - h]$ . For  $j \in \{\ell, r\}$  it holds in  $(\mathcal{D}_{\mathbb{R}}[h, T - h], d_{\parallel, \cdot})$  as  $n \rightarrow \infty$  almost surely  $(\hat{\mu}_j)_t \rightarrow (\tilde{\mu}_j)_t$ ,  $(\hat{\sigma}_j^2)_t \rightarrow (\tilde{\sigma}_j^2)_t$  and  $(\hat{\nu}_j^2)_t \rightarrow (\tilde{\nu}_j^2)_t$ , with estimators in (8) and limit functions in (19) and (20).*

The Lemma is based on a functional strong law of large numbers combining the populations left and right of  $c$ . It extends Lemma 4.1 that states consistency for the population parameters if  $C = \emptyset$ . We state the limits. They constitute non-random functions in  $t$  which in the neighborhood of  $c$  depend on the parameters of both populations. The dependence

on  $t$  and  $h$  is omitted and the tilde notation differentiates from the time-constant population parameters. If  $C = \{c\}$  then  $\mathbf{X}$  derives from two auxiliary processes  $\mathbf{X}_u = (X_{u,i})_{i=1,2,\dots}$  for  $u \in \{1, 2\}$ , with parameters  $\mu_u$ ,  $\sigma_u^2$  and  $\nu_u^2$ . For  $j \in \{\ell, r\}$  let  $(\tilde{\vartheta}_j)_t$  denote a placeholder for the limits and let  $\vartheta_1$  and  $\vartheta_2$  denote the associated parameters, e.g., choose  $\tilde{\mu}_\ell$  together with  $\mu_1$  and  $\mu_2$ , also see Figure 7. Recall the left window  $(t-h, t]$  and the right window  $(t, t+h]$ .

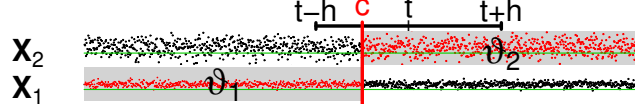


Figure 7: Decomposition for  $C = \{c\}$ . The left window  $(t-h, t]$  decomposes into  $(t-h, c]$  referring to  $\mathbf{X}_1$  and  $(c, t]$  referring to  $\mathbf{X}_2$ . The right window  $(t, t+h]$  entirely refers to  $\mathbf{X}_2$ .

For both  $j \in \{\ell, r\}$  we differentiate two cases: first, when the window does not overlap  $c$ , then all involved RVs refer to a single auxiliary process  $\mathbf{X}_u$  and the limit equals the underlying population parameter

$$\tilde{\vartheta}_\ell := \begin{cases} \vartheta_1, & t < c, \\ \vartheta_2, & t \geq c+h, \end{cases} \quad \text{and} \quad \tilde{\vartheta}_r := \begin{cases} \vartheta_1, & t < c-h, \\ \vartheta_2, & t \geq c, \end{cases} \quad (19)$$

e.g., for time  $t$  in Figure 7 it is  $\tilde{\vartheta}_r = \vartheta_2$ , in accordance with Lemma 4.1. Second, if the window overlaps  $c$ , then the limit depends on the parameters of both populations, see left window in Figure 7. Set  $\tilde{\vartheta}_\ell$  for  $t \in [c, c+h)$  as

$$\begin{aligned} \tilde{\mu}_\ell &:= \frac{c-(t-h)}{h}\mu_1 + \frac{t-c}{h}\mu_2 \\ \tilde{\sigma}_\ell^2 &:= \frac{c-(t-h)}{h}[\sigma_1^2 + (\tilde{\mu}_\ell - \mu_1)^2] + \frac{t-c}{h}[\sigma_2^2 + (\tilde{\mu}_\ell - \mu_2)^2] \\ \tilde{\nu}_\ell^2 &:= \left( \frac{c-(t-h)}{h}[\mu_1^{\{4\}} - 4\mu_1^{\{3\}}(\tilde{\mu}_\ell - \mu_1) + 6\sigma_1^2(\tilde{\mu}_\ell - \mu_1)^2 + (\tilde{\mu}_\ell - \mu_1)^4] \right. \\ &\quad \left. + \frac{t-c}{h}[\mu_2^{\{4\}} - 4\mu_2^{\{3\}}(\tilde{\mu}_\ell - \mu_2) + 6\sigma_2^2(\tilde{\mu}_\ell - \mu_2)^2 + (\tilde{\mu}_\ell - \mu_2)^4] \right) - \tilde{\sigma}_\ell^4, \end{aligned} \quad (20)$$

and define  $\tilde{\vartheta}_r$  for  $t \in [c-h, c)$  by replacing in (20) first all subscripts  $\ell$  with  $r$  and second  $t$  with  $t+h$ . We comment on (20) considering the left window  $(t-h, t]$ . Note that a proportion of  $[c-(t-h)]/h$  RVs belongs to  $\mathbf{X}_1$  and the remainder  $(t-c)/h$  refers to  $\mathbf{X}_2$ . The first order  $\tilde{\mu}_\ell$  describes a linear interpolation between  $\mu_1$  and  $\mu_2$ . The higher orders are additionally affected by the first order  $\tilde{\mu}_\ell$  via  $(\tilde{\mu}_\ell - \mu_u)^k$  with  $k \in \{1, 2, 4\}$ . For example in  $\tilde{\sigma}_\ell^2$  we find  $\sigma_u^2$  and additionally  $(\tilde{\mu}_\ell - \mu_u)^2$  and the latter is interpreted as error that derives from  $\hat{\sigma}_\ell^2 = (1/nh) \sum_{i \in I_\ell} (X_i - \hat{\mu}_\ell)^2$  as a consequence of the mean  $\hat{\mu}_\ell$  being calculated from all RVs in the window  $(t-h, t]$  violating  $c$ . All errors vanish  $(\tilde{\mu}_\ell - \mu_u)^k = 0$ , iff the expectation is constant  $\mu_1 = \mu_2 = \tilde{\mu}_\ell$ . Lemma 7.2 extends directly to multiple change points separated by at least  $h$ .

We now define the centering  $(j_{h,t}^{(n)})_t$  via  $j_{h,t}^{(n)} := (e_{h,t}^{(n)}, v_{h,t}^{(n)})^t$  and

$$e_{h,t}^{(n)} := \frac{\tilde{\mu}_r - \tilde{\mu}_\ell}{[(\tilde{\sigma}_r^2 + \tilde{\sigma}_\ell^2)/(nh)]^{1/2}} \quad \text{and} \quad v_{h,t}^{(n)} := \frac{\tilde{\sigma}_r^2 - \tilde{\sigma}_\ell^2}{[(\tilde{\nu}_r^2 + \tilde{\nu}_\ell^2)/(nh)]^{1/2}}, \quad (21)$$

using the limits from (19) and (20). The structure of  $e_{h,t}^{(n)}$  and  $v_{h,t}^{(n)}$  inherits from  $E_{h,t}^{(n)}$  and  $V_{h,t}^{(n)}$ , see (5). We focus on the inside of the  $h$ -neighborhood of  $c$  and discuss  $(e_{h,t})_t$  and  $(v_{h,t})_t$  w.r.t. the type of the change.

First we discuss  $(e_{h,t})_t$ , see Figure 6B. Message 1: a constant expectation results in vanishing  $(e_{h,t})_t$ , see green function. This is because  $\mu_1 = \mu_2$  implies  $\tilde{\mu}_\ell = \tilde{\mu}_r$  see (20), regardless of changes in higher moments. Thus,  $(E_{h,t})_t$  is robust against changes in moments of higher order than the expectation. Message 2: a change in expectation causes a systematic deviation of  $(e_{h,t})_t$  from zero, see red or light blue functions. Thus,  $(E_{h,t})_t$  is sensitive to changes in expectation. Since  $\tilde{\mu}_j$  describes a linear interpolation between  $\mu_1$  and  $\mu_2$ , the difference  $\tilde{\mu}_r - \tilde{\mu}_\ell$  takes the form of a hat that has its peak at  $c$  and this hat shape is additionally affected through the scaling  $(\tilde{\sigma}_r^2 + \tilde{\sigma}_\ell^2)^{1/2}$ .

Now we discuss  $(v_{h,t})_t$ , see Figure 6C. Here the situation is more complex as there are higher moments involved and a change in expectation affects the estimation of the higher moments. Message 1: a constant expectation results in an analog interpretation of  $(v_{h,t})_t$  as that of  $(e_{h,t})_t$ : first, a constant variance has no impact on  $(v_{h,t})_t$ . This is because for  $\mu_1 = \mu_2$  and  $\sigma_1^2 = \sigma_2^2$  we find  $\tilde{\sigma}_\ell^2 = \tilde{\sigma}_r^2$ , see (20). Second, a change in variance causes a systematic deviation from zero, see green function. This is because for  $\mu_1 = \mu_2$  we find that  $\tilde{\sigma}_j^2$  describes a linear interpolation between  $\sigma_1^2$  and  $\sigma_2^2$ , such that the difference  $\tilde{\sigma}_r^2 - \tilde{\sigma}_\ell^2$  takes the form of a hat which is affected through the scaling  $(\tilde{\nu}_r^2 + \tilde{\nu}_\ell^2)^{1/2}$ . This means that  $(V_{h,t})_t$  is sensitive to changes in the variance and robust against higher order changes given the expectation is unchanged. Regarding  $(j_{h,t})_t$  we mention a linear trajectory along the ordinate, see Figure 6D (green). Message 2: a change in expectation falsely results in a systematic deviation of  $(v_{h,t})_t$  from zero even if the variance is constant, see red perturbation. This is because  $\tilde{\sigma}_r^2 \neq \tilde{\sigma}_\ell^2$  which is caused by the errors  $(\tilde{\mu}_r - \mu_u)^2$  and  $(\tilde{\mu}_\ell - \mu_u)^2$ , see (20). This bias is also present at the third change point that causes the light blue function, though it is not as obvious as besides the change in expectation there is also a change in variance. Thus,  $(V_{h,t})_t$  is not robust against changes in the expectation.

We state the remaining functions of (18). We set  $(\Delta_{h,t}^{(n)})_t$  and  $(\tilde{D}_{h,t})_t$  as

$$\Delta_{h,t}^{(n)} := \begin{pmatrix} \Delta_{h,t,1}^{(n)} & 0 \\ 0 & \Delta_{h,t,2}^{(n)} \end{pmatrix} \quad \text{and} \quad \tilde{D}_{h,t} := \begin{pmatrix} \tilde{D}_{h,t,1} & 0 \\ 0 & \tilde{D}_{h,t,2} \end{pmatrix}, \quad (22)$$

with  $\Delta_{h,t,1}^{(n)} := [(\tilde{\sigma}_r^2 + \tilde{\sigma}_\ell^2)/(\hat{\sigma}_r^2 + \hat{\sigma}_\ell^2)]^{1/2}$  and  $\Delta_{h,t,2}^{(n)} := [(\tilde{\nu}_r^2 + \tilde{\nu}_\ell^2)/(\hat{\nu}_r^2 + \hat{\nu}_\ell^2)]^{1/2}$  as well as  $\tilde{D}_{h,t,1} := \lim_{n \rightarrow \infty} [(\tilde{\sigma}_r^2 + \tilde{\sigma}_\ell^2)/(nh\text{Var}(\hat{\mu}_r - \hat{\mu}_\ell))]^{1/2}$  and  $\tilde{D}_{h,t,2} := \lim_{n \rightarrow \infty} [(\tilde{\nu}_r^2 + \tilde{\nu}_\ell^2)/(nh\text{Var}(\hat{\sigma}_r^2 - \hat{\sigma}_\ell^2))]^{1/2}$ .

The factor  $(\Delta_{h,t}^{(n)})_t$  replaces the limits of the estimators with the actual estimators. It extends  $\Delta_{h,c}^{(n)}$  from (16). Lemma 7.2 implies  $(\Delta_{h,t}^{(n)})_t \rightarrow (I)_t$  a.s. componentwise as  $n \rightarrow \infty$ . The factor  $(\tilde{D}_{h,t})_t$  replaces the limits with the true asymptotic standard deviations of the numerators in  $J_{h,t}^{(n)}$  and thus preserves an asymptotic variance of unity in both components. It can be interpreted as the amount of inconsistency in parameter estimation caused by  $c$ . Outside the  $h$ -neighborhood of  $c$  it is  $\tilde{D}_{h,t} = I$  and also at  $c$  it is  $\tilde{D}_{h,c} = I$ . This means consistency and we note that each window entirely refers to a single auxiliary process. In Figure 6IIID we see that in the red section the joint process lies very close to  $(j_{h,t})_t$  but slightly shifted away systematically. This is because we actually had to distort  $(j_{h,t})_t$  with the factor  $(\tilde{D}_{h,t})_t$ . We comment on the variance of  $\hat{\mu}_\ell$ : if  $(t - h, t]$  does not overlap  $c$  then  $nh\text{Var}(\hat{\mu}_\ell)$  tends to  $\sigma_u^2$  as  $n \rightarrow \infty$ . If it overlaps  $c$  then it tends to the weighted average



$[(c - (t - h))/h]\sigma_1^2 + [(t - c)/h]\sigma_2^2$ , and we mention the absence of the additional error  $(\tilde{\mu}_\ell - \mu_1)^2$  as compared to  $\hat{\sigma}_\ell^2$  in (20):  $nh\text{Var}(\hat{\mu}_\ell)$  respects for  $c$  while the estimator  $\hat{\sigma}_\ell^2$  does not.

Finally, we mention that  $(\mathcal{L}_{h,t}^*)_t$  resembles  $(\mathcal{L}_{h,t})_t$  from (9) in many regards, particularly they are both Gaussian processes with  $N_2(0, I)$  distributed marginals. They differ only in the temporal covariance (not the covariance between the components): inside the  $h$ -neighborhood of  $c$  the temporal covariance of  $(\mathcal{L}_{h,t}^*)_t$  is affected by the population parameters, while outside  $(\mathcal{L}_{h,t}^*)_t$  and  $(\mathcal{L}_{h,t})_t$  both write as in (9).

## 8 Practical Performance

We discuss practical aspects of the method. First, we extend it to simultaneous application of multiple windows in Subsection 8.1. This improves the detection of change points on multiple time scales and with different effects. In Subsection 8.2 we discuss the companion R-package `jcp`. Then, in Subsection 8.3 we show simulation studies under  $C = \emptyset$ . Particularly we find that the asymptotic significance level  $\alpha$  of the test is kept in many scenarios. In Subsection 8.4 we discuss simulations studies in case of  $C \neq \emptyset$ . We show reliable detection accuracy and adequate interpretation. Finally, we give a real data example in Subsection 8.5.

### 8.1 Extension to multiple windows

We extend the test from Section 5 and the algorithm from Section 6 and consider multiple windows simultaneously. For  $\mathbf{X} \in \mathcal{M}$  consider a set  $H$  of increasingly ordered window sizes  $h_1 < \dots < h_w$  satisfying (4), which yields multiple processes  $\{(J_{h,t})_t \mid h \in H\}$ . The rational is that first, smaller windows are more sensitive to change points that appear fast in time, as they tend to avoid overlap of adjacent change points, which preserves an unbiased excursion of the joint process and thus supports detection precision. Second, larger windows improve the detection of small effects, as the associated dartboard at the change point is shifted outwards with order  $\sqrt{nh}$ , compare Lemma 6.2.

We extend the test. Recall the convergence of the temporal maximum  $M_h^{(n)}(\Gamma)$  under  $C = \emptyset$ , see (12). This maximum is associated with a single window  $h$ , but the convergence extends when additionally the maximum over all windows  $h \in H$  is considered. Continuous mapping implies for  $n \rightarrow \infty$

$$M^{(n)}(\Gamma) := \max_h M_h^{(n)}(\Gamma) \xrightarrow{d} \max_h \max_t d_I(\mathcal{L}_{h,t}). \quad (23)$$

We use  $M(\Gamma) := M^{(1)}(\Gamma)$  as a global test statistic and reject iff it exceeds the  $(1 - \alpha)$ -quantile  $Q$  of the distribution of the right hand side. Again we approximate  $Q$  in simulations. We can treat  $\Gamma$  analogously to the single window case, compare table 1: first, symmetry assumption yields  $\Gamma = I$  and results in the Euclidean distance  $d_I$ . Second, consistent estimation  $\hat{\Gamma}$  of  $\Gamma$  results in the Mahalanobis distance  $d_{\hat{\Gamma}}$ , while  $\hat{\Gamma}$  depends on  $t$  due to the local estimation but now also on  $h$ , see (13). Third, we can be conservative and omit  $\Gamma$  by considering the maximum distance  $d_\infty$ . Thinking in terms of the joint processes we now derive a rejection region  $\mathcal{R}$  such that any of the involved joint processes enters  $\mathcal{R}$  only with probability  $\alpha$ , if  $C = \emptyset$ . In the first case we find  $\mathcal{R} = \mathcal{C}^c$  while  $\mathcal{C}$  is the circle with radius  $Q$ . In the second case we find  $\mathcal{R} = \hat{\mathcal{C}}^c$  with  $\hat{\mathcal{C}} = \hat{\Gamma}^{1/2} \cdot \mathcal{C}$  and due to the dependence of  $\hat{\Gamma}$  on  $t$  and  $h$  we consider a separate time dependent ellipse  $\hat{\mathcal{C}}$  for any involved joint process. In the third case it is

$\mathcal{R} = \mathcal{S}^c$  while  $\mathcal{S}$  is a square with center zero and edge length  $2Q$ . To make the dependence on  $H$  explicit we write  $\mathcal{R}(H)$ .

If the null hypothesis is rejected we aim at detecting change points. We use a bottom-up approach similar to Messer et al. (2014). First detect candidates  $\hat{C}_{h_k}$  from every window size  $h_k$ . Then combine all candidates into a final set  $\hat{C}$  favoring smaller over larger windows.

**Algorithm 8.1.** Set  $\mathcal{R}(H)$  as either  $\mathcal{C}^c$ ,  $\hat{\mathcal{C}}^c$  or  $\mathcal{S}^c$  as used in the test. For each  $h_k \in H$  obtain  $\hat{C}_{h_k}$  using Algorithm 6.1 w.r.t.  $\mathcal{R}(H)$ . Set  $\hat{C} := \hat{C}_{h_1}$ . For increasing  $k = 2, 3, \dots$  update  $\hat{C}$  as follows: add any  $\hat{c} \in \hat{C}_{h_k}$  to  $\hat{C}$  that satisfies  $\{\hat{c} - h_k + 1, \dots, \hat{c} + h_k\} \cap \hat{C} = \emptyset$ .

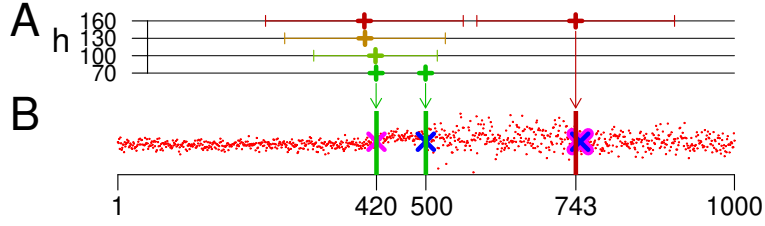


Figure 8: Depiction of the multi window algorithm. B: Process  $\mathbf{X} \in \mathcal{M}$ ,  $T = 1000$ , change points  $C = \{420, 500, 750\}$  (crosses, magenta = change in expectation, blue = change in variance),  $N(\mu, \sigma^2)$ -distributed RVs, four sections with  $\mu = 2, 10, 10, 4$  and  $\sigma = 4, 4, 12, 8$ . Rejection region  $\mathcal{R}(H) = \mathcal{C}^c$ ,  $\alpha = 0.05$ . Final estimates  $\hat{C} = \{420, 500, 743\}$  (vertical bars). A: four windows  $H = \{70, 100, 130, 160\}$  (light green to dark red), candidates  $\hat{C}_{h_k}$  (+ symbols), their  $h_k$ -neighborhoods (colored horizontal lines). Algorithm: first set  $\hat{C} := \hat{C}_1 = \{420, 500\}$ , next dismiss  $\hat{C}_2 = \{419\}$  and  $\hat{C}_3 = \{402\}$ , finally from  $\hat{C}_4 = \{401, 743\}$  only accept 743 for  $\hat{C}$ . The colors of the bars in B indicate the window associated with the acceptance (twice light green and once dark red).

A candidate from the  $k$ -th step is dismissed if a previously accepted estimate falls into the candidates  $h_k$ -neighborhood. The algorithm is shown in Figure 8. Three change points are present and three estimates are obtained. Note that any  $\hat{C}_{h_k}$  contains two estimates at the most – the small windows lack power to detect the small effect at the last change point, while the larger windows are not sensitive to the first two change points that occur fast.

## 8.2 The jcp-package

The method is made available in the R-package `jcp` (*joint change point detection*) on CRAN. It also contains a summary and a plotting routine. For the example of Figure 8 it generates Figure 9.

In A we see the input  $\mathbf{X}$ . The null hypotheses  $C = \emptyset$  is rejected. The bars mark the three estimates  $\hat{C}$ . B visualizes empirical means ( $\approx 2.1, 11.3, 10.3, 5.4$ ) and standard deviations ( $\approx 4.0, 4.2, 11.7, 8.5$ ) calculated from all data within the estimated sections: the plus marks the estimation from all data left of the first estimate 420. Then the outgoing arrow directs right, meaning an increase in the mean at 420. The second arrow points upwards (and slightly left) meaning an increase in standard deviation at 500. Finally, the last arrow points south-west meaning a decline in both estimates at 743. The lengths of the arrows indicate the strengths of the effects. Segment C facilitates change point interpretation, extending the explanation from Section 6: assuming symmetric data we find a rejection circle. The four involved processes  $(J_{h,t})_t$  are omitted to avoid visual overload. The legend explains the color coding of the windows. The effect at the first estimated change point 420 is strong: it is the

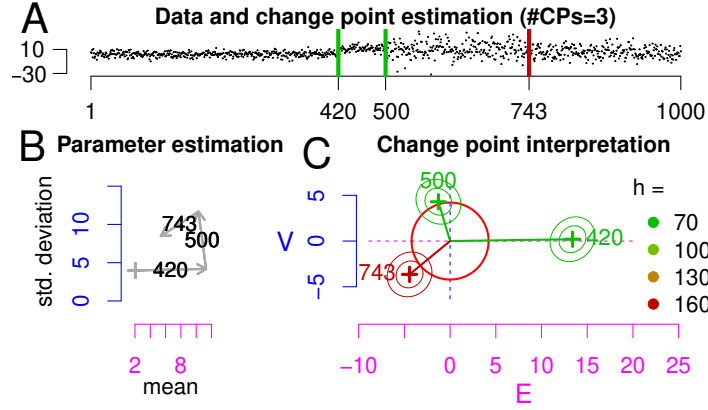


Figure 9: Plotting routine of the R-package jcp.

smallest window  $h_1 = 70$  that detects the change and the dartboard lies far away from zero. Since the dartboard touches the abscissa, it is not hard to argue that the change occurred in expectation only. The effect at the second estimate 500 is less strong. However, the dartboard is light green, i.e., it was still the smallest window to detect the change. The dartboard lies close to the ordinate and thus it is not hard to argue that the change occurred only in the variance. The third dartboard is found in dark red. The largest window  $h_4 = 160$  was necessary to detect the change. In that sense, the effect is the smallest of all (also compare the short arrow in segment B). The dartboard lies diagonally and it is now hard to argue that a change only occurred in a single parameter.

### 8.3 Significance level and window choice

**Significance level** We constructed an asymptotic test for which we let  $n \rightarrow \infty$ . We linked  $n$  to a window size  $h$  through  $nh$  which then grows. In practice however, we consider the real time scenario  $n = 1$ . Thus, for a suitable approximation of the rejection boundary we need the smallest window to be sufficiently large. By construction,  $\mathcal{R} \in \{\mathcal{C}^c, \hat{\mathcal{C}}^c\}$  results in an asymptotic level that equals a predefined  $\alpha$ , while  $\mathcal{R} = \mathcal{S}^c$  results in a reduced level, see table 1. We evaluate the rejection probability under  $C = \emptyset$  for  $n = 1$  in simulations. We will see that  $\alpha$  is kept in many parameter combinations of different distributions if the smallest window size involved is about  $h = 50$ .

In the following let  $\alpha = 0.05$ . Processes with  $T = 1000$  and  $C = \emptyset$  are simulated. The relative frequency of rejections  $f_{\mathcal{R}}$  (based on 1000 simulations) approximates the rejection probability. In Figure 10 we see  $f_{\mathcal{R}}$  depending on the window set for four different distributions,  $N(0, 1)$  (magenta),  $\exp(1)$  (green),  $\text{gamma}(p = 0.5, \lambda = 2)$  (blue) and  $\text{gamma}(2, 2)$  (red), with parameters shape  $p$  and rate  $\lambda$ . For  $N(0, 1)$  we use  $\mathcal{R} = \mathcal{C}^c$ , else we use  $\mathcal{R} = \hat{\mathcal{C}}^c$  (solid lines) or  $\mathcal{R} = \mathcal{S}^c$  (dotted lines). The window set is chosen  $H_k = \{10(1+k), 10(3+k), \dots, 10(11+k)\}$  with  $k \in \{0, 1, \dots, 15\}$ , i.e., each  $H_k$  contains six windows which are all increased by 10 when increasing  $k$ . We nicely see that  $f_{\mathcal{R}}$  tends to the true  $\alpha = 5\%$  for increasing  $k$ , if  $\mathcal{R} = \mathcal{C}^c$  or  $\hat{\mathcal{C}}^c$ . We also see that  $f_{\mathcal{R}}$  is reduced for the conservative approach  $\mathcal{R} = \mathcal{S}^c$ . Overall, the approximation is adequate for the choice of the smallest window of about 30 to 50. We mention that  $f_{\mathcal{R}}$  is overestimated when small windows  $k \in \{0, 1\}$  are involved. For an intuition consider normally distributed RVs where  $E_{h,t}^{(n)}$  (Welch's statistic) is  $t$ -distributed for fixed  $n$ , while its limit is  $N(0, 1)$  distributed. But as the  $t$ -distribution has heavier tails than

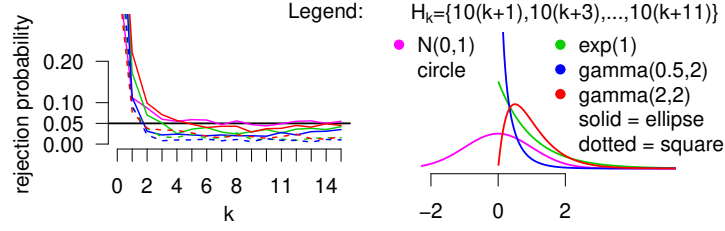


Figure 10: Left: Simulated rejection probability  $f_{\mathcal{R}}$  (1000 simulations each), depending on  $H_k = \{10(1+k), 10(3+k), \dots, 10(11+k)\}$  with  $k \in \{0, 1, \dots, 15\}$ .  $T = 1000$ ,  $C = \emptyset$ ,  $\alpha = 5\%$ . Four distributions color coded:  $N(0,1)$  with  $\mathcal{R} = \mathcal{C}^c$  (magenta). Also  $\exp(1)$  (green),  $\gamma(0.5,2)$  (blue) and  $\gamma(2,2)$  (red) with  $\mathcal{R} = \mathcal{E}^c$  (solid) or  $\mathcal{R} = \mathcal{S}^c$  (dotted). Right: Legend.

$N(0,1)$ , especially for  $n$  small,  $E_{h,t}^{(n)}$  is more likely to take a large value as compared to the limit marginal used for the derivation of the threshold.

The previous analysis suggests that the  $\alpha$ -level is kept for a smallest window of about 50 for the four distributions considered. This holds true for many other parameters: in Figure 11 we see  $f_{\mathcal{R}}$  for a fixed window set  $H = \{50, 75, 100, 125, 150\}$  depending on the expectation  $\mu$  and the standard deviation  $\sigma$  of the underlying distribution,  $N(\mu, \sigma^2)$  with  $\mathcal{R} = \mathcal{C}^c$  (A), and  $\gamma(p, \lambda)$  with  $\mathcal{R} = \mathcal{E}^c$  (B) or  $\mathcal{R} = \mathcal{S}^c$  (C), mentioning  $p = \mu^2/\sigma^2$  and  $\lambda = \mu/\sigma^2$ . We find  $f_{\mathcal{R}}$  color-coded according to the legend in A: green means 5%, while red indicates higher, and blue lower rejection probabilities. For  $N(\mu, \sigma^2)$  we choose  $\mu \in \{-3, -2, \dots, 3\}$  and

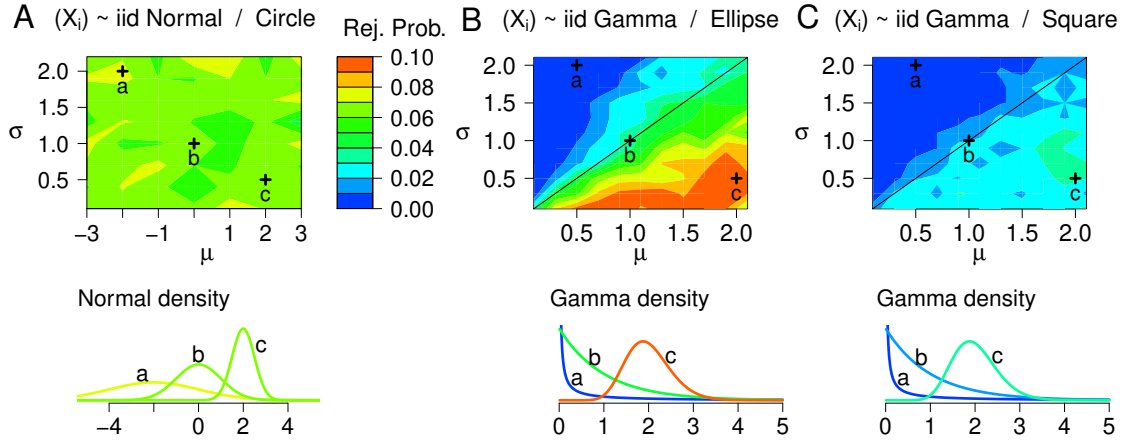


Figure 11: Upper panels: simulated rejection probability  $f_{\mathcal{R}}$  (1000 simulations each),  $C = \emptyset$ ,  $\alpha = 5\%$ , depending on first  $\mu$  and  $\sigma$  (expectation and std. dev.), second the choice of  $\mathcal{R}$ . It is  $T = 1000$ ,  $H = \{50, 75, 100, 125, 150\}$ . A:  $N(\mu, \sigma^2)$ ,  $\mathcal{R} = \mathcal{C}^c$ . B,C:  $\gamma(p, \lambda)$ ,  $\mathcal{R} = \mathcal{E}^c$  (B), and  $\mathcal{R} = \mathcal{S}^c$  (C). Simulated probabilities color-coded according to the legend in A. For each scenario three pairs of parameters  $(\mu, \sigma)$  are marked (crosses  $a, b, c$ ) and the associated densities are shown in the lower panels (those in B and C coincide).

$\sigma \in \{0.1, 0.4, 0.7, \dots, 2.2\}$  ( $7 \cdot 8 = 56$  combinations). We find an almost entirely green picture, i.e.,  $f_{\mathcal{R}}$  is close to the true  $\alpha = 5\%$  for most combinations. For the gamma distribution we used  $\mu, \sigma \in \{0.1, 0.3, 0.5, \dots, 2.1\}$  ( $11^2 = 121$  combinations). In B  $f_{\mathcal{R}}$  varies with the parameters. For the exponential distribution  $\mu = \sigma$  (diagonal line),  $f_{\mathcal{R}}$  is about 5% while it decreases above the diagonal (small  $\mu$ , large  $\sigma$ ) and it increases below (large  $\mu$ , small  $\sigma$ ) but with  $f_{\mathcal{R}} < 10\%$  even in the most extreme case. Below the diagonal the distribution is more

bell-shaped, while  $f_{\mathcal{R}}$  is larger in B than in A. A major difference is that in B for  $\mathcal{R} = \hat{\mathcal{E}}^c$  the estimator  $\hat{\Gamma}$  additionally increases variability. In C the visual pattern is similar to B as the same distributions are considered, but overall it is colored more blue with  $f_{\mathcal{R}}$  below 3.7% throughout, and this global decrease aligns with the conservative nature of  $\mathcal{R} = \mathcal{S}^c$ .

**Window choice** We comment on the choice of windows  $H$ . For that we investigate the dependence of the rejection quantile  $Q$  on  $H$ . Recall that  $Q$  is the  $(1 - \alpha)$ -quantile of the limit distribution in (23). We set  $\alpha = 0.05$ . The radii in Figure 12 show simulations of  $Q$  (also denoted as  $Q$ ,  $10^6$  simulations).

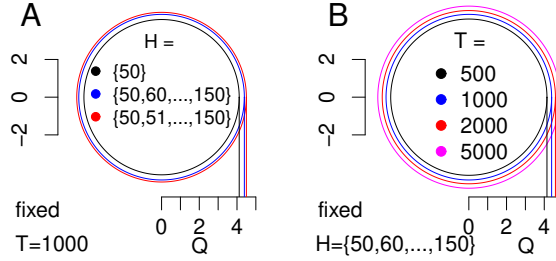


Figure 12: Dependence of  $Q$  ( $10^6$  simulations) on  $H$  for fixed  $T = 1000$  (A), and on  $T$  for fixed  $H$  (B), for  $\alpha = 0.05$ . Both blue circles coincide.

In Figure 12A there are three sets of windows compared for  $T = 1000$ : first the single window  $H_1 = \{50\}$  results in  $Q_1 \approx 4.12$  (black), second the eleven windows  $H_2 = \{50, 60, 70, \dots, 150\}$  yield  $Q_2 \approx 4.39$  (blue) and third the 101 windows  $H_3 = \{50, 51, 52, \dots, 150\}$  result in  $Q_3 \approx 4.5$  (red). We mention monotonicity:  $H_A \subset H_B$  implies  $Q_A < Q_B$  which follows from the global maximization over all windows in (23). But we also mention a flattening in the increase, i.e.,  $Q_2 - Q_1$  (black to blue) is larger than  $Q_3 - Q_2$  (blue to red) although there are much more windows added when going from blue to red. The reason for the flattening is that in (23), among all  $h \in H$  the processes  $(\mathcal{L}_{h,t})_t$  are functionals of a single planar Brownian motion which implies  $\mathcal{L}_{h_a,t} \approx \mathcal{L}_{h_b,t}$  for  $h_a \approx h_b$  with equality if  $h_a = h_b$ . Thus, if  $H$  constitutes a fine grid then additional windows have minor impact on the processes' global maximum. In Figure 12B  $H = \{50, 60, \dots, 150\}$  is fixed and four choices for  $T$  are differentiated. For  $T_1 = 500$  we obtain  $Q_1 \approx 4.14$  (black),  $T_2 = 1000$  yields  $Q_2 \approx 4.39$  (blue - same setup as in A),  $T_3 = 2000$  yields  $Q_3 \approx 4.6$  (red) and  $T_4 = 5000$  results in  $Q_4 \approx 4.83$  (magenta). Again, we mention monotonicity:  $T_A < T_B$  implies  $Q_A < Q_B$ . This is because in (23) the processes  $(\mathcal{L}_{h,t})_t$  are evaluated for  $t \in [h, T - h]$  i.e., for larger  $T$  the maxima are taken over longer time periods.

Regarding the choice of  $H$  we now argue that first, the richer the combination of windows the better a scenario of unknown change points and effects is exploited: for  $c \in C$  we find  $h \in H$  preferably large such that  $(c - h, c + h]$  is free from other change points resulting in an unbiased excursion of the joint process, see Proposition 7.1 and Lemma 6.2. The order of the excursion is  $\sqrt{h}$ , while the competitor  $Q$  is bounded (for fixed  $T$  and  $\alpha$ ) through the quantile associated with all windows possible. Second, as discussed in Subsection 8.3, the smallest window should be chosen large enough, e.g., 50, such that the significance level of the test is approximately kept.

#### 8.4 Performance evaluation

For  $C \neq \emptyset$  we evaluate the detection performance in simulation studies. We show precise estimation of the number and the location of change points, and appropriate interpretation of the effects. The results are shown in Figure 13 and 14. We differentiate first normally distributed RVs using  $\mathcal{R} = \mathcal{C}^c$  (left) and second gamma distributed RVs with  $\mathcal{R} = \mathcal{S}^c$  (right). It is  $T = 1000$ ,  $\alpha = 5\%$ , and  $C = \{c_1, c_2, c_3\}$  with a change only in expectation at  $c_1$  (magenta cross), a change only in variance at  $c_2$  (blue cross), and change in both at  $c_3$  (magenta and blue cross), see **X** in A. We perform 1000 simulations i.e., in total there are 3000 true change points involved. We classify an estimate  $\hat{c}$  as correct if its distance to a true change point is 25 at the most (arbitrary criterion). The 25-neighborhood of a true change point is accentuated by a gray box. Statistics of  $\hat{c}$  are color-coded according to the associated true change point (red = first, green = second or light blue = third change point, black = classified incorrect).

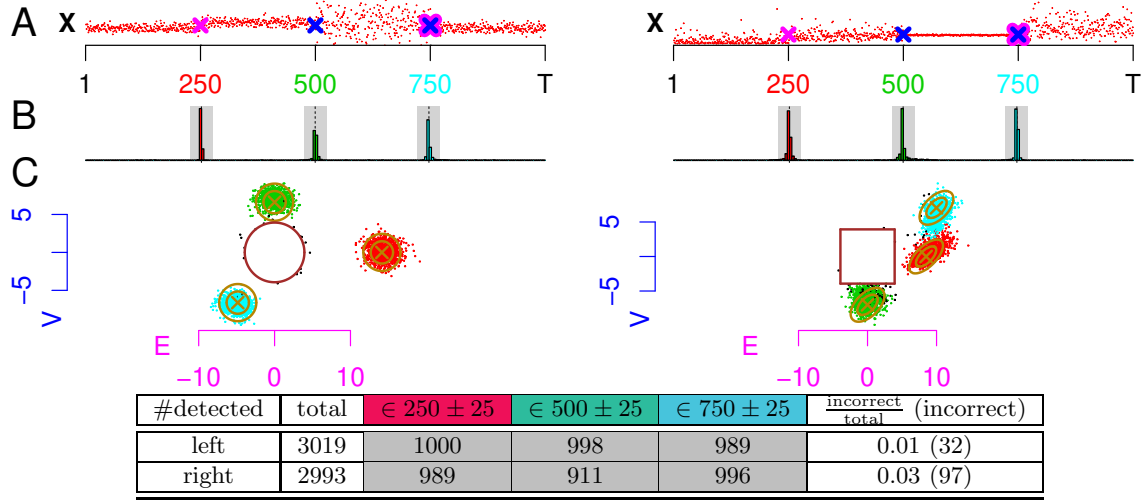


Figure 13: Performance evaluation.  $T = 1000$ ,  $H = \{100\}$ ,  $C = \{250, 500, 750\}$  and  $\alpha = 0.05$ . Left: normal distribution,  $\mu = 2, 10, 10, 2$ ,  $\sigma = 4, 4, 16, 4$ ,  $\mathcal{R} = \mathcal{C}^c$ . Right: gamma distribution,  $\mu = 0.8, 2, 2, 4$ ,  $\sigma = 1, 1, 0.1, 2$ ,  $\mathcal{R} = \mathcal{S}^c$ . A: Process **X**, B: Distribution of change points estimates, color-coded:  $\hat{c}$  in  $250 \pm 25$  red, in  $500 \pm 25$  green, in  $750 \pm 25$  light blue, else colored black. C: Underlying  $J_{h,\hat{c}}$  (points) colored to match  $\hat{c}$  in B, golden: asymptotic distribution of  $J_{h,c}$  for true  $c \in C$ , brown: rejection boundaries.

In Figure 13 we consider a single window  $h = 100$  and  $C = \{250, 500, 750\}$ . B shows the distribution of the estimates  $\hat{C}$ : we see three narrow histograms around the true change points which supports estimation precision. The frequencies are shown in the table, e.g., left the total number of detected change points is  $|\hat{C}| = 3019$ . All of the thousand true change points at 250 were detected with a distance of at most 25 (red histogram). For 250 we find 998 (green) and for the 750 we find 989 (light blue histogram) estimates in the gray boxes. Only 32 estimates are found outside the boxes (black, hardly visible due to low number). Segment C shows  $J_{h,\hat{c}}$  for all  $\hat{c} \in \hat{C}$ , i.e., the local maximal values of  $(J_{h,t})_t$  whose arguments constitute  $\hat{C}$ . E.g., left we find 998 green points. The statistics  $J_{h,\hat{c}}$  distribute closely to the golden dartboards which visualize the asymptotic distribution of  $J_{h,c}$  for  $c \in C$ . Thus, interpretation of effects based on  $J_{h,\hat{c}}$  is plausible in practice: e.g., from a typical red point it is not hard to argue that the associated change occurred only in the expectation. We also see

32 black points which refer to those estimates classified incorrect: some lie close to the brown rejection boundary and are considered real false positives resulting from chance. In contrast some black points lie in the area of the dart boards and thus refer to true change points being classified as incorrect due to the widths 25 of the gray boxes, i.e., they represent the tails of the histograms in B.

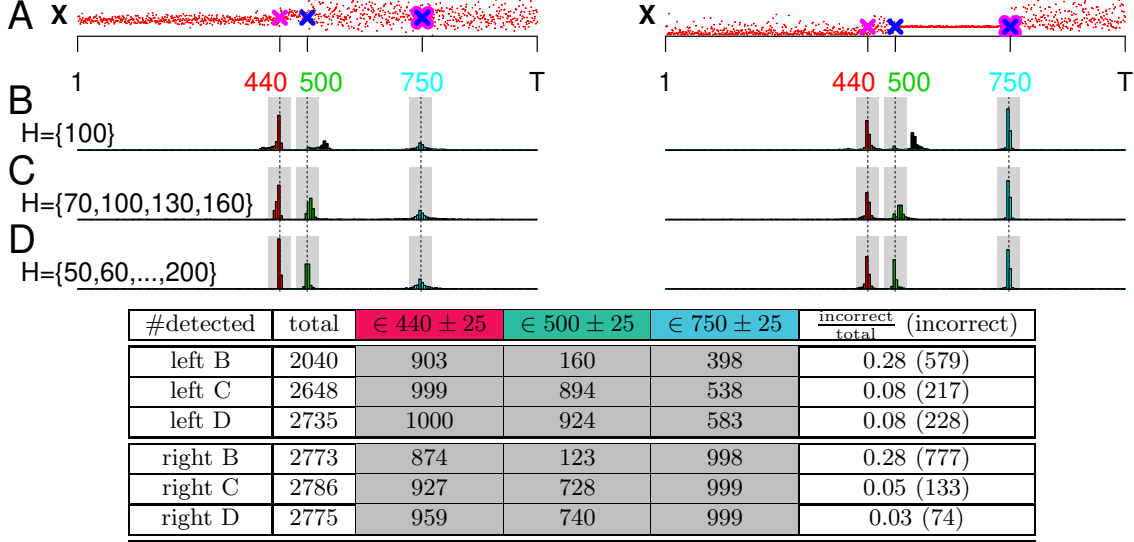


Figure 14: Performance evaluation.  $T = 1000$ ,  $C = \{440, 500, 750\}$ ,  $\alpha = 0.05$ , for  $H = \{100\}$  (B),  $H = \{70, 100, 130, 160\}$  (C) and  $H = \{50, 60, \dots, 200\}$  (D). Left: normal distribution,  $\mu = 2, 10, 10, 6$ ,  $\sigma = 4, 4, 12, 10$ ,  $\mathcal{R} = \mathcal{C}^c$ . Right: gamma distribution,  $\mu = 0.8, 2, 2, 4$ ,  $\sigma = 1, 1, 0.1, 2$ ,  $\mathcal{R} = \mathcal{S}^c$ . A: Process  $\mathbf{X}$ . B, C, D: Distribution of change points estimates, color-coded:  $\hat{c}$  in  $250 \pm 25$  red, in  $500 \pm 25$  green, in  $750 \pm 25$  light blue, else colored black.

In summary, the method showed great performance. However, the setup was well-disposed as change points  $C$  are separated sufficiently and effects were chosen strong enough, i.e., the fixed window  $h = 100$  generates enough power to shift a dartboard far out. To further prove detection performance we choose three change points  $C = \{440, 500, 750\}$ , the first two lying closer together now, see Figure 14. For the normal distribution (left) we also reduced the effects. We differentiate three sets of windows  $H_1 = \{100\}$  (B),  $H_2 = \{70, 100, 130, 160\}$  (C) and  $H_3 = \{50, 60, \dots, 200\}$  (D). Performance improves when window set increases: first, the table shows an increase in the number of detections (almost throughout), while the relative proportion of estimates classified as incorrect reduces. Second, separately investigating the three true change points, the number of estimates classified as correct increases. Third, B, C and D show improvement in location precision as the estimates distribute more narrow around the true change points.

## 8.5 Data example

We consider the weekly production of albumen in Canada, observed from Sep. 1980 to Dec. 1997 as reported by Statistics Canada (table 32-10-0133-01, report of processed eggs production). This makes  $T = 900$  time stamps and the data (unit  $10^3 kg$ ) is depicted in Figure 15A. We set  $\alpha = 0.05$ ,  $\mathcal{R} = \mathcal{S}^c$  and  $H = \{50, 70, 90, 110, 130\}$ . The null hypothesis  $C = \emptyset$  was rejected. Five change points were detected  $\hat{C} = \{125, 227, 382, 643, 811\}$ . Visually, the



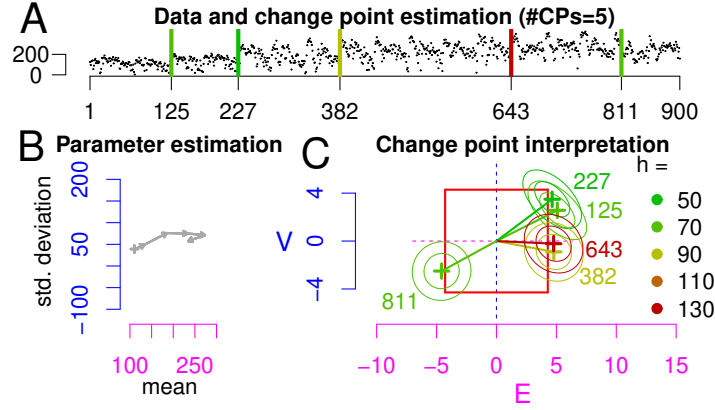


Figure 15: Data example. Canadian production of albumen ( $\times 10^3$  kg), weekly in 1980 - 1997.

segmentation seems reasonable. From Figure 15C we conclude that the estimates at 382 and 643 indicate an increase in expectation, those at 125 and 227 an increase in both expectation and variance and at 811 a decrease in both quantities.

## 9 Discussion

We proposed a method for change point detection in univariate sequences. Data is modeled as independent RVs that are piecewise identically distributed. To jointly detect changes in expectation and variance we developed a bivariate moving sum approach: a comparison of empirical means in adjacent windows is sensitive to changes in expectation, and a comparison of empirical variances is suitable for the detection of changes in variance. Methodologically, first an asymptotic test was constructed to test the null hypothesis that no change occurred. Second, an algorithm for change point detection was presented, that can be applied if the null hypothesis is rejected.

The method is grounded on the asymptotic behavior of the moving sum process. Under the null hypothesis it was shown to approach a zero mean Gaussian process from which the rejection boundary of the test was derived in simulations. Under the alternative it asymptotically describes a Gaussian process that systematically deviates from zero locally around a change point. The quantification of this deviation supported the sensitivity of the moving sum process to change points. The first component was shown to be sensitive to changes in expectation and robust against higher order changes. The second component was shown to be sensitive to changes in variance, but unfortunately it also reacts to changes in expectation. Importantly, it is the joint consideration of both components that supports adequate estimation. Inference on the strength of a change (effect size) as well as its type (expectation, variance, or both) is enabled with confidence.

The bivariate process was classified according to the presence or absence of symmetry of the underlying distribution. Symmetry, on the one hand was shown to result in independent asymptotic components and is thus related to Euklid's notion of distance: under the null hypothesis symmetry results first in the isotropy of the moving sum process and thus in a rejection area given by a circle. Second in case of change points, we found the marginals at the change points to be asymptotically uncorrelated, depicted by round contour lines. On the other hand, a lack of symmetry of the underlying distribution was shown to result in



correlated components of the moving sum process, and is therefore related to Mahalanobis' notion of distance: first, under the null hypothesis the moving sum process was shown to have a preferred direction of variability along the main diagonals in  $\mathbb{R}^2$ , which results in an elliptic rejection boundary. Second, the marginals at the change points were shown to have correlated components, resulting in elliptic contour lines. We presented three ways to treat the unknown correlation in applications: first, symmetry assumption results in vanishing correlation. Second, correlation can be estimated consistently. Third, a conservative approach that avoids to address correlation was presented.

The method was further extended to improve the detection of change points on different scales. For that, multiple bivariate moving sum processes were applied simultaneously. Indeed, various simulation studies revealed strong performance under different distributional assumptions, like the normal, exponential or gamma distribution, in case of both the presence or absence of change points. Generally, weak distributional assumptions allow for wide ranging applications, for which we mention that all methodology developed relates to true statistics in the sense that there are no unknown parameters remaining. The method is ready to use and implemented in the R package `jcp`, which performs the test and the algorithm, summarizes the results and provides a graphical output to facilitate interpretation.

## 10 Appendix

We give here all proofs.

**Proof of Lemma 4.1:** We show the convergences for the left window half,  $j = \ell$ . First note that both estimators  $\hat{\sigma}_\ell^2$  and  $\hat{\nu}_\ell^2$  from (8) decompose into the sum of empirical moments. An elementary calculus gives  $\hat{\sigma}_\ell^2 = \hat{\mu}_\ell^{(2)} - \hat{\mu}_\ell^2$  and  $\hat{\nu}_\ell^2 = \hat{\mu}_\ell^{(4)} - 4\hat{\mu}_\ell\hat{\mu}_\ell^{(3)} + 8\hat{\mu}_\ell^2\hat{\mu}_\ell^{(2)} - 2(\hat{\mu}_\ell^{(2)})^2 - 4\hat{\mu}_\ell^4$ . Thus, it suffices to show almost sure process convergence of the empirical moments to the constant processes given by the theoretical moments, i.e.,  $(\hat{\mu}_\ell^{(k)})_t \rightarrow (\mu^{(k)})_t$  a.s. For that, we first show that in  $(\mathcal{D}_\mathbb{R}[0, T], d_{\|\cdot\|})$  it holds almost surely as  $n \rightarrow \infty$

$$\left( \frac{1}{n} \sum_{i=1}^{\lfloor nt \rfloor} X_i^k \right)_t \longrightarrow (t\mu^{(k)})_t \quad (24)$$

We discretize time to apply the strong law of large numbers. We bound

$$\begin{aligned} \sup_{0 \leq t \leq T} \left| \frac{1}{n} \sum_{i=1}^{\lfloor nt \rfloor} X_i^k - t\mu^{(k)} \right| &\leq \sup_{0 \leq t \leq T} \left| \frac{1}{n} \sum_{i=1}^{\lfloor nt \rfloor} X_i^k - \frac{\lfloor nt \rfloor}{n} \mu^{(k)} \right| + r_n \\ &= \max_{m \in \{1, 2, \dots, nT\}} \left| \frac{1}{n} \sum_{i=1}^m X_i^k - \frac{m}{n} \mu^{(k)} \right| + r_n, \end{aligned}$$

with remainder  $r_n := \sup_{t \in [0, T]} |t - \lfloor nt \rfloor/n| \mu^{(k)} \leq (1/n) \mu^{(k)}$ . We find  $r_n \rightarrow 0$  as  $n \rightarrow \infty$  and also show that the maximum tends to zero almost surely. Let  $\varepsilon > 0$ . For almost every realization we find  $m_0 \in \mathbb{N}$  such that  $|(1/m) \sum_{i=1}^m X_i^k - \mu^{(k)}| < \varepsilon/2$  for all  $m > m_0$ , according

to the strong law or large numbers. But then we bound

$$\begin{aligned} & \max_{m \in \{1, 2, \dots, nT\}} \left| \frac{1}{n} \sum_{i=1}^m X_i^k - \frac{m}{n} \mu^{(k)} \right| \\ & \leq \frac{1}{n} \max_{m \leq m_0} \left| \sum_{i=1}^m X_i^k - m \mu^{(k)} \right| + \frac{m}{n} \max_{m_0 < m \leq nT} \left| \frac{1}{m} \sum_{i=1}^m X_i^k - \mu^{(k)} \right| \leq \varepsilon \end{aligned}$$

for  $n$  sufficiently large, since the maximum in the first summand is independent from  $n$  and the maximum of the second summand becomes small according to the strong law of large numbers. Because  $\varepsilon$  can be chosen arbitrarily small the left hand side tends to zero almost surely and (24) holds. From that we conclude that in  $(\mathcal{D}_{\mathbb{R}}[h, T-h], d_{\|\cdot\|})$  it holds a.s. as  $n \rightarrow \infty$

$$\begin{aligned} (\hat{\mu}_\ell^{(k)})_t &= \left( \frac{1}{nh} \sum_{i=1}^{\lfloor nt \rfloor} X_i^k \right)_t - \left( \frac{1}{nh} \sum_{i=1}^{\lfloor n(t-h) \rfloor} X_i^k \right)_t \\ &\rightarrow \left( \frac{t}{h} \mu^{(k)} \right)_t - \left( \frac{t-h}{h} \mu^{(k)} \right)_t = (\mu^{(k)})_t, \end{aligned}$$

which yields the statement.  $\square$

**Proof of Proposition 4.2:** We define the standardized variables  $Y_i := (X_i - \mu)/\sigma$  and  $\mathcal{Y}_i := [(X_i - \mu)^2 - \sigma^2]/\nu$  on which we apply a bivariate functional central limit theorem and obtain convergence to a planar Brownian motion. In  $(\mathcal{D}_{\mathbb{R}^2}[0, T], d_{SK})$  it holds as  $n \rightarrow \infty$

$$\left[ \frac{1}{\sqrt{n}} \Gamma^{-1/2} \cdot \begin{pmatrix} \sum_{i=1}^{\lfloor nt \rfloor} Y_i \\ \sum_{i=1}^{\lfloor nt \rfloor} \mathcal{Y}_i \end{pmatrix} \right]_t \xrightarrow{d} \begin{pmatrix} W_t \\ \mathcal{W}_t \end{pmatrix}_t, \quad (25)$$

see e.g., Kuelbs (1973). Then we define a continuous map  $\varphi = (\varphi_1, \varphi_2)^t$  from  $(\mathcal{D}_{\mathbb{R}^2}[0, T], d_{SK})$  to  $(\mathcal{D}_{\mathbb{R}^2}[h, T-h], d_{SK})$  via

$$\varphi_\kappa : (f_\kappa(t))_t \rightarrow \left( \frac{[f_\kappa(t+h) - f_\kappa(t)] - [f_\kappa(t) - f_\kappa(t-h)]}{\sqrt{2h}} \right)_t$$

for both components  $\kappa = 1, 2$ . Applying  $\varphi$  on (25) yields in  $(\mathcal{D}_{\mathbb{R}^2}[h, T-h], d_{SK})$  as  $n \rightarrow \infty$

$$\left[ \Gamma^{-1/2} \cdot \begin{pmatrix} (2\sigma^2 nh)^{-1/2} \left[ \sum_{i \in I_r} X_i - \sum_{i \in I_\ell} X_i \right] \\ (2\nu^2 nh)^{-1/2} \left[ \sum_{i \in I_r} (X_i - \mu)^2 - \sum_{i \in I_\ell} (X_i - \mu)^2 \right] \end{pmatrix} \right]_t \xrightarrow{d} (\mathcal{L}_{h,t})_t,$$

while the centering terms  $\mu$  and  $\sigma^2$  cancel out in both components. In the second component we now replace  $\mu$  with the local estimator  $\hat{\mu}_j$  which yields

$$\left[ \Gamma^{-1/2} \cdot \begin{pmatrix} (\hat{\mu}_r - \hat{\mu}_\ell) / \sqrt{2\sigma^2/(nh)} \\ (\hat{\sigma}_r^2 - \hat{\sigma}_\ell^2) / \sqrt{2\nu^2/(nh)} \end{pmatrix} \right]_t \xrightarrow{d} (\mathcal{L}_{h,t})_t, \quad (26)$$

We comment on the replacement. For  $j \in \{\ell, r\}$  we find

$$\begin{aligned} & \frac{1}{\sqrt{nh}} \sum_{i \in I_j} (X_i - \mu)^2 \\ &= \frac{1}{\sqrt{nh}} \sum_{i \in I_j} (X_i - \hat{\mu}_j)^2 - 2(\hat{\mu}_j - \mu) \frac{1}{\sqrt{nh}} \sum_{i \in I_j} (X_i - \mu) + \frac{1}{\sqrt{nh}} nh [\hat{\mu}_j - \mu]^2. \end{aligned}$$

The second summand of the r.h.s. vanishes uniformly over  $t$  almost surely as  $n \rightarrow \infty$  according to Slutsky's Lemma, as first from Lemma 4.1 we obtain  $(\hat{\mu}_j)_t \rightarrow (\mu)_t$  a.s., and second we have weak process convergence for  $[(nh)^{-1/2} \sum_{i \in I_j} (X_i - \mu)]_t$  to a Gaussian process limit as a consequence of the square-root scaling. The third summand is  $-1/2$  of the second summand and thus also vanishes uniformly almost surely. Thus, the weak functional limit of the l.h.s. and the first summand of the r.h.s. are equal due to Slutsky's Lemma, which yields (26). Finally, Lemma 4.1 also states the almost sure convergence of  $(\hat{\sigma}_j^2)_t \rightarrow (\sigma^2)_t$  and  $(\hat{\nu}_j^2)_t \rightarrow (\nu^2)_t$  for  $j \in \{\ell, r\}$  such that  $2\sigma^2$  and  $2\nu^2$  in (26) can be replaced by  $\hat{\sigma}_r^2 + \hat{\sigma}_\ell^2$  and  $\hat{\nu}_r^2 + \hat{\nu}_\ell^2$  again according to Slutsky's Lemma, which is the statement.  $\square$

**Proof of Lemma 6.2:** We introduce

$$D_{h,c}^{(n)} := \sqrt{nh} \cdot \left( \frac{(\hat{\mu}_r - \hat{\mu}_\ell) - (\mu_2 - \mu_1)}{(\sigma_2^2 + \sigma_1^2)^{1/2}}, \frac{(\hat{\sigma}_2^2 - \hat{\sigma}_1^2) - (\sigma_2^2 - \sigma_1^2)}{(\nu_2^2 + \nu_1^2)^{1/2}} \right)^t, \quad (27)$$

which is different from  $J_{h,c}^{(n)}$  in two aspects: first, by centering the numerators, the change point is taken into account, and consequently preserves convergence. Second, the true order of scaling is used in the denominators instead of the estimators. Then we can write  $J_{h,c}^{(n)} - \Delta_{h,c}^{(n)} \cdot j_{h,c}^{(n)} = \Delta_{h,c}^{(n)} \cdot D_{h,c}^{(n)}$ . From Lemma 4.1 it follows that  $\Delta_{h,c}^{(n)} \rightarrow I$  almost surely by components as  $n \rightarrow \infty$ , such that it remains to show that  $D_{h,c}^{(n)} \xrightarrow{d} N_2(0, \Gamma_c)$ . The idea is to apply the multivariate  $\delta$ -method to the quadruple  $(\hat{\mu}_r, \hat{\sigma}_r^2, \hat{\mu}_\ell, \hat{\sigma}_\ell^2)^t$  the latter of which the multivariate central limit theorem holds true. Note that we operate on a triangular scheme when letting  $n \rightarrow \infty$  such that we apply Lindeberg's version of the latter. Since the components with subscript  $\ell$  are independent from those with subscript  $r$ , we obtain as  $n \rightarrow \infty$

$$\sqrt{nh} \left[ \begin{pmatrix} \hat{\mu}_r \\ \hat{\sigma}_r^2 \\ \hat{\mu}_\ell \\ \hat{\sigma}_\ell^2 \end{pmatrix} - \begin{pmatrix} \mu_2 \\ \sigma_2^2 \\ \mu_1 \\ \sigma_1^2 \end{pmatrix} \right] \xrightarrow{d} N_4(0, \Sigma) \quad \text{with} \quad \Sigma = \begin{pmatrix} \sigma_2^2 & \mu_2^{\{3\}} & 0 & 0 \\ \mu_2^{\{3\}} & \nu_2^2 & 0 & 0 \\ 0 & 0 & \sigma_1^2 & \mu_1^{\{3\}} \\ 0 & 0 & \mu_1^{\{3\}} & \nu_1^2 \end{pmatrix},$$

compare also (1). We define a differentiable map  $\Phi : \mathbb{R}^4 \rightarrow \mathbb{R}^2$  via  $(x_2, y_2, x_1, y_1)^t \xrightarrow{\Phi} (x_2 - x_1, y_2 - y_1)^t$ . Then the Jacobian matrix  $J$  of  $\Phi$  writes as

$$J = \begin{pmatrix} 1 & 0 & -1 & 0 \\ 0 & 1 & 0 & -1 \end{pmatrix}.$$

By  $\delta$ -method we obtain as  $n \rightarrow \infty$  that

$$\sqrt{nh} \left( \begin{pmatrix} \hat{\mu}_r - \hat{\mu}_\ell \\ \hat{\sigma}_r^2 - \hat{\sigma}_\ell^2 \end{pmatrix} - \begin{pmatrix} \mu_2 - \mu_1 \\ \sigma_2^2 - \sigma_1^2 \end{pmatrix} \right) \xrightarrow{d} N_2(0, \Sigma^*) \quad \text{with} \\ \Sigma^* = J \Sigma J^t = \begin{pmatrix} \sigma_2^2 + \sigma_1^2 & \mu_2^{\{3\}} + \mu_1^{\{3\}} \\ \mu_2^{\{3\}} + \mu_1^{\{3\}} & \nu_2^2 + \nu_1^2 \end{pmatrix}.$$

But this yields as  $n \rightarrow \infty$

$$D_{h,c}^{(n)} = \sqrt{nh} \begin{pmatrix} (\sigma_2^2 + \sigma_1^2)^{-1/2} & 0 \\ 0 & (\nu_2^2 + \nu_1^2)^{-1/2} \end{pmatrix} \left( \begin{pmatrix} \hat{\mu}_r - \hat{\mu}_\ell \\ \hat{\sigma}_r^2 - \hat{\sigma}_\ell^2 \end{pmatrix} - \begin{pmatrix} \mu_2 - \mu_1 \\ \sigma_2^2 - \sigma_1^2 \end{pmatrix} \right) \xrightarrow{d} N_2(0, \Gamma_c),$$

since  $\Gamma_c = D\Sigma^*D^t$ , while  $D$  denotes the diagonal matrix of the latter display.  $\square$

**Proof of Lemma 7.2:** We explain why  $\tilde{\mu}_j$  is the almost sure limit of the estimator  $\hat{\mu}_j = (1/nh) \sum_{i \in I_j} X_i$ . We discuss the left window  $(t-h, t]$ , i.e.,  $j = \ell$ . The asymptotics of  $\hat{\mu}_\ell$  depend on the location of  $c$  relative to the window. We already know a.s. convergence to the population parameter if the  $c$  is not overlapped. If  $c$  lies within the window, we decompose  $(t-h, t] = (t-h, c] \cup (c, t]$ . The lengths of these subintervals relative to the window size  $h$  give the proportions of random variables of both auxiliary processes: regarding  $\hat{\mu}_\ell$  we obtain a.s. as  $n \rightarrow \infty$

$$\begin{aligned} \hat{\mu}_\ell = & \left[ \frac{nc - \lfloor n(t-h) \rfloor}{nh} \frac{1}{nc - \lfloor n(t-h) \rfloor} \sum_{i=\lfloor n(t-h) \rfloor + 1}^{nc} X_{1,i} \right] \\ & + \left[ \frac{\lfloor nt \rfloor - nc}{nh} \frac{1}{\lfloor nt \rfloor - nc} \sum_{i=nc+1}^{\lfloor nt \rfloor} X_{2,i} \right] \longrightarrow \frac{c - (t-h)}{h} \mu_1 + \frac{t-c}{h} \mu_2. \end{aligned} \quad (28)$$

The convergence of  $\hat{\mu}_r$  to  $\tilde{\mu}_r$  follows analogously. This pointwise consideration for all  $t$  extends to uniform convergence with analogous arguments as in Lemma 4.1, mainly making use of the functional strong law of large numbers in (24). For  $\hat{\sigma}_j^2$ ,  $\hat{\nu}_j^2$  and  $\hat{\mu}^{\{3\}}$  we also exemplary focus on the left window with decompose  $(t-h, t] = (t-h, c] \cup (c, t]$ . We replace the summands  $X_{u,i}$  in (28). For  $\hat{\sigma}_\ell^2$  we obtain three summands  $(X_{u,i} - \hat{\mu}_\ell)^2 = (X_{u,i} - \mu_u)^2 - 2(X_{u,i} - \mu_u)(\hat{\mu}_\ell - \mu_u) + (\hat{\mu}_\ell - \mu_u)^2$ , which yields e.g., for the left subinterval where  $u = 1$ , almost surely as  $n \rightarrow \infty$

$$\frac{1}{nc - \lfloor n(t-h) \rfloor} \sum_{i=\lfloor n(t-h) \rfloor + 1}^{nc} (X_{1,i} - \hat{\mu}_\ell)^2 \longrightarrow \sigma_1^2 + (\tilde{\mu}_\ell - \mu_1)^2,$$

while the mean of the first summand  $(X_{1,i} - \mu_1)^2$  tended to  $\sigma_1^2$ , the mean of the second summand  $-2(X_{1,i} - \mu_1)(\hat{\mu}_\ell - \mu_1)$  vanished since  $(\hat{\mu}_\ell - \mu_1)$  does not depend on the summation, and because the mean of  $X_{1,i}$  tends to  $\mu_1$ . And for the same reason we found the mean of the third summand  $(\hat{\mu}_\ell - \mu_1)^2$  to converge to  $(\tilde{\mu}_\ell - \mu_1)^2$ , using also that  $\hat{\mu}_\ell$  tends to  $\tilde{\mu}_\ell$ . For  $\hat{\nu}_\ell^2 = \hat{\mu}_\ell^{\{4\}} - \hat{\sigma}_\ell^4$  it remains to comment on the asymptotics of  $\hat{\mu}_\ell^{\{4\}}$  while in the decomposition (28) we obtain five summands  $(X_{u,i} - \hat{\mu}_\ell)^4 = (X_{u,i} - \mu_u)^4 - 4(X_{u,i} - \mu_u)^3(\hat{\mu}_\ell - \mu_u) + 6(X_{u,i} - \mu_u)^2(\hat{\mu}_\ell - \mu_u)^2 - 4(X_{u,i} - \mu_u)(\hat{\mu}_\ell - \mu_u)^3 + (\hat{\mu}_\ell - \mu_u)^4$ , and for the left subinterval we find a.s. as  $n \rightarrow \infty$

$$\begin{aligned} & \frac{1}{nc - \lfloor n(t-h) \rfloor} \sum_{i=\lfloor n(t-h) \rfloor + 1}^{nc} (X_{1,i} - \hat{\mu}_\ell)^4 \\ & \longrightarrow \mu_1^{\{4\}} - 4\mu_1^{\{3\}}(\tilde{\mu}_\ell - \mu_1) + 6\sigma_1^2(\tilde{\mu}_\ell - \mu_1)^2 + (\tilde{\mu}_\ell - \mu_1)^4, \end{aligned}$$

while the fourth summand vanished as the mean of  $X_{u,i}$  tends to  $\mu_u$  a.s. Finally, regarding  $\hat{\mu}_\ell^{\{3\}}$  we obtain four summands in (28) as  $(X_{u,i} - \hat{\mu}_\ell)^3 = (X_{u,i} - \mu_u)^3 - 3(X_{u,i} - \mu_u)^2(\hat{\mu}_\ell - \mu_u) + 3(X_{u,i} - \mu_u)(\hat{\mu}_\ell - \mu_u)^2 - (\hat{\mu}_\ell - \mu_u)^3$ , and for the left subinterval we find a.s. as  $n \rightarrow \infty$

$$\frac{1}{nc - \lfloor n(t-h) \rfloor} \sum_{i=\lfloor n(t-h) \rfloor + 1}^{nc} (X_{1,i} - \hat{\mu}_\ell)^3 \longrightarrow \mu_u^{\{3\}} - 3\sigma_1^2(\tilde{\mu}_r - \mu_1) - (\tilde{\mu}_r - \mu_1)^3,$$

while the third summand vanished, again because the mean of  $X_{u,i}$  tends to  $\mu_u$  a.s.  $\square$

**Proof of Proposition 7.1:** By construction of  $\mathbf{X}$  having a single change point  $c$ , there are two independent auxiliary processes  $\mathbf{X}_1$  and  $\mathbf{X}_2$  involved, having population parameters  $\mu_u$ ,  $\sigma_u^2$  and  $\nu_u^2$ , for  $u \in \{1, 2\}$ . Again, we define the standardized variables  $Y_{u,i} := (X_{u,i} - \mu_u)/\sigma_u$  and  $\mathcal{Y}_{u,i} := [(X_{u,i} - \mu_u)^2 - \sigma_u^2]/\nu_u$ , for which we apply the bivariate functional central limit theorem. For  $u \in \{1, 2\}$  it holds in  $(\mathcal{D}_{\mathbb{R}^2}[0, T], d_{SK})$  as  $n \rightarrow \infty$

$$\left[ \frac{1}{\sqrt{n}} \left( \sum_{i=1}^{\lfloor nt \rfloor} Y_{u,i} \right) \right] \xrightarrow{d} \left( \begin{matrix} W_{u,t} \\ \mathcal{W}_{u,t} \end{matrix} \right)_t, \quad (29)$$

while the right hand side describes a planar Brownian motion. The inverse root  $\Gamma_u^{-1/2}$  writes as the identity  $I$  since  $\rho_u = 0$ . The independence of the two auxiliary processes  $\mathbf{X}_1$  and  $\mathbf{X}_2$  inherits to the two planar Brownian motions for  $u = 1$  and  $2$ . This also results in the joint convergence, i.e.,  $u = 1$  and  $2$ , of the two bivariate processes on the left hand side of (29). We replace the scaling  $\sigma_u$  and  $\nu_u$  of the random variables with the asymptotics of the estimators  $(\tilde{\sigma}_r^2 + \tilde{\sigma}_\ell^2)^{1/2}$  and  $(\tilde{\nu}_r^2 + \tilde{\nu}_\ell^2)^{1/2}$ , see (19) and (20), and further scale with  $h^{1/2}$  which yields in  $(\mathcal{D}_{\mathbb{R}^2}[h, T-h], d_{SK})$  as  $n \rightarrow \infty$

$$\left[ \frac{1}{\sqrt{nh}} \left( \begin{matrix} [\sigma_u/(\tilde{\sigma}_r^2 + \tilde{\sigma}_\ell^2)^{1/2}] \sum_{i=1}^{\lfloor nt \rfloor} Y_{u,i} \\ [\nu_u/(\tilde{\nu}_r^2 + \tilde{\nu}_\ell^2)^{1/2}] \sum_{i=1}^{\lfloor nt \rfloor} \mathcal{Y}_{u,i} \end{matrix} \right) \right] \xrightarrow{d} \left[ \frac{1}{\sqrt{h}} \left( \begin{matrix} [\sigma_u/(\tilde{\sigma}_r^2 + \tilde{\sigma}_\ell^2)^{1/2}] \cdot W_{u,t} \\ [\nu_u/(\tilde{\nu}_r^2 + \tilde{\nu}_\ell^2)^{1/2}] \cdot \mathcal{W}_{u,t} \end{matrix} \right) \right]_t, \quad (30)$$

We now consider joint convergence for  $u = 1, 2$ , i.e., pointwise we operate on  $\mathbb{R}^4$ . To switch to the moving sum perspective, we define a continuous map  $\varphi : (\mathcal{D}_{\mathbb{R}^2}[h, T-h] \times \mathcal{D}_{\mathbb{R}^2}[h, T-h], d_{SK} \otimes d_{SK}) \rightarrow (\mathcal{D}_{\mathbb{R}^2}[h, T-h] \times \mathcal{D}_{\mathbb{R}^2}[h, T-h], d_{SK} \otimes d_{SK})$ . For that we write an element from the domain of  $\varphi$  as  $r := [((f_1, f_2)(t))_t, ((g_1, g_2)(t))_t]$ , with  $f_\kappa$  associated with the  $\kappa$ -th component of the first process ( $u = 1$ ), and  $g_\kappa$  with the  $\kappa$ -th component of the second process ( $u = 2$ ), for  $\kappa = 1, 2$ . Then we define  $\varphi = (\varphi_1, \varphi_2)$  componentwise for  $\kappa = 1, 2$  identical via

$$\varphi_\kappa(r) := \left( \begin{matrix} [(f_\kappa(t+h) - f_\kappa(t)) - (f_\kappa(t) - f_\kappa(t-h))] \mathbb{1}_{[h, c-h)}(t) \\ + [(g_\kappa(t+h) - g_\kappa(c)) + (f_\kappa(c) - f_\kappa(t)) - (f_\kappa(t) - f_\kappa(t-h))] \mathbb{1}_{[c-h, c)}(t) \\ + [(g_\kappa(t+h) - g_\kappa(t)) - (g_\kappa(t) - g_\kappa(c)) - (f_\kappa(c) - f_\kappa(t-h))] \mathbb{1}_{[c, c+h)}(t) \\ + [(g_\kappa(t+h) - g_\kappa(t)) - (g_\kappa(t) - g_\kappa(t-h))] \mathbb{1}_{[c+h, T-h]}(t) \end{matrix} \right)_t.$$

The mapping takes the  $\kappa$ -th component in (30) and connects – in the sense of the moving sum statistic – the process left of the change point  $u = 1$ , with the process right from the change point  $u = 2$ . Continuous mapping preserves convergence. The first and the fourth summand refer to points in time outside the  $h$ -neighborhood of  $c$  that refer to a single auxiliary process  $\mathbf{X}_1$ , respectively  $\mathbf{X}_2$ . For those points the mapping directly results in  $(J_{h,t})_t \xrightarrow{d} (\mathcal{L}_{h,t})_t$ , as in Proposition 4.2. For that we recall that the  $\tilde{\sigma}_j^2$  and  $\tilde{\nu}_j^2$  equal the population parameters  $\sigma_u^2$  and  $\nu_u^2$ . We need to discuss behavior inside the  $h$ -neighborhood of  $c$ . We focus on the case that  $c$  lies in the right window  $t \in [c-h, c)$ , and consider the first component  $\kappa = 1$ . The second component follows with analogous arguments. If we apply  $\varphi_1$  on the left hand side of (30) we obtain

$$\begin{aligned} \sqrt{nh} \left[ \frac{1}{nh} \left( \sum_{i=\lfloor nc \rfloor+1}^{\lfloor n(t+h) \rfloor} X_{i,2} + \sum_{i=\lfloor nt \rfloor+1}^{\lfloor nc \rfloor} X_{i,1} \right) - \frac{1}{nh} \sum_{i=\lfloor n(t-h) \rfloor+1}^{\lfloor nt \rfloor} X_{i,1} \right] \\ - \sqrt{nh} \left[ \frac{[(t+h)-c]\mu_2 - (c-t)\mu_1}{(\tilde{\sigma}_r^2 + \tilde{\sigma}_\ell^2)^{1/2}} \right] \\ = \sqrt{nh} \frac{\hat{\mu}_r - \hat{\mu}_\ell}{\sqrt{\tilde{\sigma}_r^2 + \tilde{\sigma}_\ell^2}} - \sqrt{nh} \frac{\tilde{\mu}_r - \tilde{\mu}_\ell}{\sqrt{\tilde{\sigma}_r^2 + \tilde{\sigma}_\ell^2}}. \end{aligned} \quad (31)$$

For the right hand side of (30) we get

$$\frac{\sigma_2(W_{t+h,2} - W_{c,2}) - \sigma_1[(W_{c,1} - W_{t,1}) - (W_{t,1} - W_{t-h,1})]}{\sqrt{(\tilde{\sigma}_r^2 + \tilde{\sigma}_\ell^2)h}}. \quad (32)$$

Finally, we replace the scaling using Slutsky's Lemma. First, by multiplication of (31) with the first diagonal entry of  $\Delta_{h,t}^{(n)}$  we replace the scaling  $(\tilde{\sigma}_r^2 + \tilde{\sigma}_\ell^2)^{1/2}$  with the estimators  $(\hat{\sigma}_r^2 + \hat{\sigma}_\ell^2)^{1/2}$ , while the limit remains the same as  $\Delta_{h,t}^{(n)} \rightarrow (I)_t$  a.s. Second, by multiplication of both sides (31) and (32) with the first diagonal entry of  $(\tilde{D}_{h,t})_t$  we scale to unit variance, and we also mention that (32) has zero expectation. Without changing the law we can replace the two Brownian motions by a single Brownian motion  $(W_t)_t$  such that the resulting process is continuous. This gives the first component of  $(\mathcal{L}_{h,t}^*)_t$ . Convergence of the second component follows analogously, noting that the functional  $\varphi_2$  equals  $\varphi_1$ . Consequently, the limit exhibits the same properties as the limit of the first component. Finally, also joint convergence to  $(\mathcal{L}_{h,t}^*)_t$  having independent components inherits from (29).  $\square$

## References

- Adler, R. J. (1990). An introduction to continuity, extrema, and related topics for general gaussian processes. Lecture Notes-Monograph Series, 12:i-155.
- Albert, S., Messer, M., Schiemann, J., Roeper, J., and Schneider, G. (2017). Multi-scale detection of variance changes in renewal processes in the presence of rate change points. J Time Ser Anal.
- Albin, J. M. P. (1990). On extremal theory for stationary processes. Ann. Probab., 18(1):92-128.
- Aston, J. A. D. and Kirch, C. (2012). Evaluating stationarity via change-point alternatives with applications to fmri data. Ann. Appl. Stat., 6(4):1906-1948.
- Aue, A. and Horváth, L. (2013). Structural breaks in time series. J Time Ser Anal, 34(1):1-16.
- Basseville, M. and Nikiforov, I. (1993). Detection of Abrupt Changes: Theory and Application. Prentice Hall Information and System Sciences Series. Prentice Hall Inc., Englewood Cliffs, NJ.
- Braun, J. V., Braun, R. K., and Muller, H. G. (2000). Multiple changepoint fitting via quasilielihood, with application to dna sequence segmentation. Biometrika, 87(2):301-314.
- Brodsky, B. (2017). Change-point analysis in nonstationary stochastic models. CRC Press, Boca Raton, FL.
- Brodsky, B. E. and Darkhovsky, B. S. (1993). Nonparametric methods in change-point problems, volume 243 of Mathematics and its Applications. Kluwer Academic Publishers, Dordrecht.
- Chen, J. and Gupta, A. K. (1997). Testing and locating variance changepoints with application to stock prices. J Am Stat Assoc, 92(438):739-747.

- Chen, J. and Gupta, A. K. (2000). Parametric statistical change point analysis. Birkhäuser Boston, Inc., Boston, MA.
- Csörgö, M. and Horváth, L. (1997). Limit theorems in change-point analysis. Wiley Series in Probability and Statistics. John Wiley & Sons, Chichester. With a foreword by David Kendall.
- Dette, H., Wu, W., and Zhou, Z. (2015). Change point analysis of second order characteristics in non-stationary time series. [arXiv:1503.08610](#).
- Eichinger, B. and Kirch, C. (2018). A mosum procedure for the estimation of multiple random change points. Bernoulli, 24(1):526–564.
- Frick, K., Munk, A., and Sieling, H. (2014). Multiscale change point inference. J R Stat Soc Series B Stat Methodol, 76(3):495–580. With 32 discussions by 47 authors and a rejoinder by the authors.
- Fryzlewicz, P. (2014). Wild binary segmentation for multiple change-point-detection. Ann Stat, 42(6):2243–2281.
- Gao, Z., Shang, Z., Du, P., and Robertson, J. L. (2018). Variance change point detection under a smoothly-changing mean trend with application to liver procurement. Journal of the American Statistical Association, 0(0):1–9.
- Horváth, L., Horváth, Z., and Hušková, M. (2008). Ratio tests for change point detection, volume Volume 1 of Collections, pages 293–304. Institute of Mathematical Statistics, Beachwood, Ohio, USA.
- Hsu, D. A. (1977). Tests for variance shift at an unknown time point. Applied Statistics, 26(3):279–284.
- Inclan, C. and Tiao, G. (1994). Use of cumulative sums of squares for retrospective detection of changes of variance. J Am Stat Assoc, 89(427):913–923.
- Jandhyala, V., Fotopoulos, S., MacNeill, I., and Liu, P. (2013). Inference for single and multiple change-points in time series. J Time Ser Anal, 34(4):423–446.
- Killick, R., Eckley, I., and Jonathan, P. (2013). A wavelet-based approach for detecting changes in second order structure within nonstationary time series. Electron J Stat, 7:1167–1183.
- Killick, R., Eckley, I. A., Ewans, K., and Jonathan, P. (2010). Detection of changes in variance of oceanographic time-series using changepoint analysis. Ocean Engineering, 37(13):1120 – 1126.
- Korkas, K. K. and Fryzlewicz, P. (2017). Multiple change-point detection for non-stationary time series using wild binary segmentation. Statist. Sinica, 27(1):287–311.
- Kuelbs, J. (1973). The invariance principle for Banach space valued random variables. J. Multivariate Anal., 3:161–172.

- Lindgren, G. (1980). Point processes of exits by bivariate gaussian processes and extremal theory for the chi-square-process and its concomitants. Journal of Multivariate Analysis, 10(2):181 – 206.
- Matteson, D. S. and James, N. A. (2014). A nonparametric approach for multiple change point analysis of multivariate data. J Am Stat Assoc, 109(505):334–345.
- Messer, M. (2019). jcp: Joint Change Point Detection. R package version 1.0.
- Messer, M., Kirchner, M., Schiemann, J., Roeper, J., Neining, R., and Schneider, G. (2014). A multiple filter test for change point detection in renewal processes with varying variance. Ann Appl Stat, 8(4):2027–2067.
- Pein, F., Sieling, H., and Munk, A. (2017). Heterogeneous change point inference. J R Stat Soc Series B Stat Methodol, 79(4):1207–1227.
- Spokoiny, V. (2009). Multiscale local change point detection with applications to value-at-risk. Ann. Statist., 37(3):1405–1436.
- Talagrand, M. (2014). Upper and lower bounds for stochastic processes, volume 60 of Ergebnisse der Mathematik und ihrer Grenzgebiete. 3. Folge. A Series of Modern Surveys in Mathematics [Results in Mathematics and Related Areas. 3rd Series. A Series of Modern Surveys in Mathematics]. Springer, Heidelberg. Modern methods and classical problems.
- van der Vaart, A. W. (1998). Asymptotic statistics, volume 3 of Cambridge Series in Statistical and Probabilistic Mathematics. Cambridge University Press, Cambridge.
- Whitcher, B., Guttorp, P., and Percival, D. (2000). Multiscale detection and location of multiple variance changes in the presence of long memory. J Stat Comput Simul, 68(1).
- Wolfe, D. A. and Schechtman, E. (1984). Nonparametric statistical procedures for the change-point problem. Journal of Statistical Planning and Inference, 9(3):389 – 396.
- Zeileis, A., Shah, A., and Patnaik, I. (2010). Testing, monitoring, and dating structural changes in exchange rate regimes. Computational Statistics & Data Analysis, 54(6):1696 – 1706.
- Zhang, H., Dantu, R., and Cangussu, J. (2009). Change point detection based on call detail records. In Intelligence and Security Informatics, 2009, pages 55–60. New York: Institute of Electrical and Electronics Engineers.